ISSN Application No. 21823

An EP Journal on Architectural Education

Volume No. 13

Issue No. 2

May - Aug 2025

ENRICHEDPUBLICATIONSPVT.LTD

S-9,IIndFLOOR,MLUPOCKET,
MANISHABHINAVPLAZA-II,ABOVEFEDERALBANK,
PLOTNO-5,SECTOR-5,DWARKA,NEWDELHI,INDIA-110075,
PHONE:-+(91)-(11)-47026006

ISSN Application No. 21823

An EP Journal on Architectural Education

Aims and Scope

An EP Journal on Architectural Education is a National Journal. It Publishes Original Research Papers in Different Areas of Architecture Education. It Publishes 3 Issues in a Year from 2018 in purpose of enhancing architectural scholarship in design, history, urbanism, cultural studies, technology, theory, and practice.

ISSN Application No. 21823

An EP Journal on Architectural Education

ISSN Application No. 21823

An EP Journal on Architectural Education

(Volume No. 13, Issue No. 2, May - Aug 2025)

Contents

ISSN Application No. 21823

Experimental Studies on Scouring Downstream of Labyrinth Weirs

A.S.Pote[1], A.D.Ghare [2]
[1]Research Scholar, Department of Civil Engineering, VNIT, Nagpur - 440010, India
[2]Associate Professor, Department of Civil Engineering, VNIT, Nagpur - 440010, India
Email: aspoteonline@gmail.com, adghare@yahoo.co.in

A B S T R A C T

Labyrinth weirs typically offer the advantage of increased effective crest length resulting in enhanced discharge for an operating head. Due to this distinct advantage, such weirs are gaining popularity. However, complex 3D flow pattern affects the nature of turbulence and the resulting scouring phenomena. Literature shows limited work on scouring patterns downstream of Labyrinth weirs. This paper presents the results of laboratory experimental study carried out to obtain the pattern and extent of scouring on the downstream side of trapezoidal plan-form labyrinth weir. These results are expected to be useful for the hydraulic engineers engaged in the task of design of labyrinth weir system.

Keywords: Labyrinth Weir, Crest Length, Scouring

1. Introduction

Scour is a natural phenomenon caused by the flow of water. It occurs when the erosive capacity of flow of water exceeds the resistance capability of earth material. Scour will continue until an equilibrium situation is reached i.e. the erosive capacity of flow becomes lower than the ability of earth material to resist it. Scour downstream hydraulic structures may result in damage or complete structural failure and loss of life and property. A labyrinth weir is an overflow weir folded in plan view to provide a longer total effective length for a given overall weir width (Figure 1). The idea of labyrinth weir is useful in increasing the discharge capacity of existing spillway economically. The idea can be traced back to 1940. The studies relating to scour patterns are even rarer. The present paper deals with the effect of various parameters of labyrinth weir, such as different aspect ratios, on the amount and pattern of downstream scour.

1.1 Literature review

Gentilini (1940) gave the initial idea of increasing discharge of weirs with a zigzag plan-form. After a hiatus of about 19 years next significant contribution was by Shalash (1959) who proposed equation for estimating scour depth downstream of weir including the effect of an apron with length L, Kotoulas

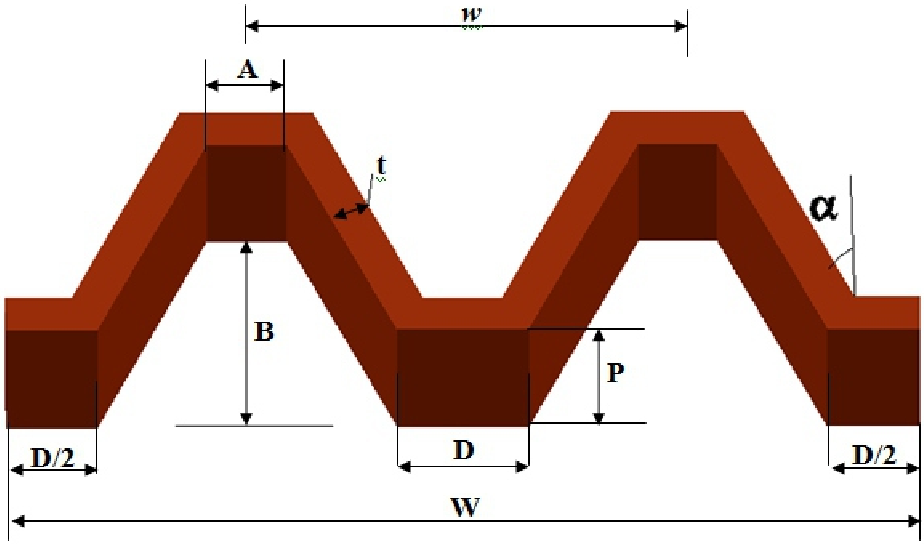

Figure 1 Layout of labyrinth weir

(1967) found that in case of coarse sand, about 64% of the final scour occurred in first 20s and about 97% of scour depth was attained in 2h. But studies for actually designing a labyrinth weir came from Taylor (1968) and Hay & Taylor (1970). Darvas (1971) gave a simplified method for design.Farthoudi and Smith(1985) studied the scour profiles downstream of a weir. Hassan and Narayanan (1985) studied the scour patterns d/s of an apron. Mason and Arumugan (1985) studied the scour caused by free jet d/s of weirs and flip buckets. Bormann (1988) defined the equilibrium scour parameters when no significant change takes place and the scour pattern becomes stable. Magalhaes & Lorena (1989) developed this method further by use of dimensionless coefficients and discharge curves. Literature on scour consists of a few studies on local scour. Bormanr & Julian (1991) contributed towards study of scour d/s of grade control structures. Whittaker and Jaggi (1996) studied the erosion d/s of labyrinth weirs. Rosgen (2001) proposed design details for eco-friendly grade control structures including W-weirs. Bijan Dargahi (2003) proposed equation for estimating maximum scour depth and rate of sediment transport by using simple power type equations that relate the scour geometry to controlling scour parameters. Bhuiyan et al.(2007) studied the flow turbulence characteristics and scour development downstream of a W-weir at river bed in clear water and live bed conditions. Pagliara (2007) studied the influence of sediment in the flow. Tullis et al (1995), (2007) Lopez et al. (2008) have made significant contribution to design methods of labyrinth weirs. The comprehensive work based on "Hydraulic design of labyrinth weirs", already published in the book by Henry Falvey (2003). Bhuiyan, Hey and Wormleaton (2007) used W-weir for river restoration and presented a hydraulic evaluation of W-weir. Moghim et al. (2008) developed an empirical equation by using regression analysis to predict the maximum scour depth downstream of apron. Khawairakpam and Muzumdar (2009) reviewed on local scour around hydraulic structures. Hossein Hamidifar (2011) performed experimental study on local scour of non-cohesive sediments downstream of a horizontal rigid apron. W-weir and other labyrinth weirs as well as other 3-D flow intervening structures are gaining in popularity for various ecological issues like river restoration, fish and habitat protection, bank protection etc. which in summarized in the work by Scurlock, Thornton and Abt.(2012). Stefano Pagliara (2014) experimentally analyzed the scour geometry downstream of rock W-weirs in straight rivers and explained the behavior of these structures in terms of scour formulations. The study of scour then becomes important as excessive scour can undermine the foundations of W-weirs and other labyrinth weirs. Estimating the possible scour in advance and using remedial measures in the construction of various labyrinth weirs, this present study will certainly be helpful in that task.

2. Experimental set up

(Figure 2) indicates the arrangement of the experimental set up used for computation of maximum scour and its pattern downstream of labyrinth weir in the present study. Experiments were conducted at the fluid mechanics laboratory of the G.H.Raisoni college of engineering and management, Pune in a tilting flume 0.35 m wide , 4 m long, and 0.5 m high. The water re-circulation arrangement was provided in the flume. The re-circulation was done through 50mm diameter pipe with the 3HP pump. At the downstream end of flume, a sump 1.5m×1.5m×0.65m was provided at the inlet, a tank of size 0.8×1.0m×0.65m was provided. For carrying out the experimental study, the labyrinth models with side wall angle $6^0, 8^0, 10^0, 16^0, 21^0$ were fabricated using 15mm think acrylic sheet. The labyrinth model in present study was provided with quarter round crest shape. Each labyrinth model consisted of two full cycles having total width of 0.3m and height 0.25m. On the upstream of the labyrinth weir, baffle walls were provided for damping the turbulence. For measurement of water surface level and sand level, vernier type gauge with 2 mm least count was used, the discharge was measured by volumetric method . During the experiments the nappe of labyrinth weir was kept well ventilated. The experiment work was started with the proper arrangement of tilting flume with zero degree slope and 10cm think sand level was prepared. Four different types of arrangements of extended length of apron on downstream of labyrinth weir were tested. At the beginning of each experiment, the sand level bed was carefully leveled. All experiments were conducted in subcritical flow condition without hydraulic jump formation. The flow rate (Q) was varied in the range of 0.00765 m^3/s to 0.01260 m^3/s.

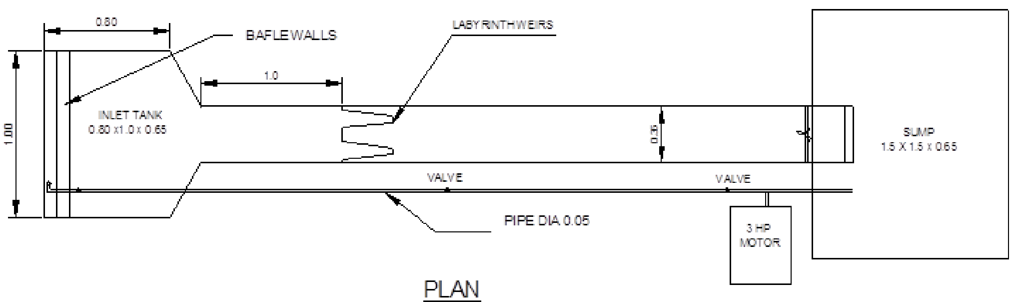

PLAN

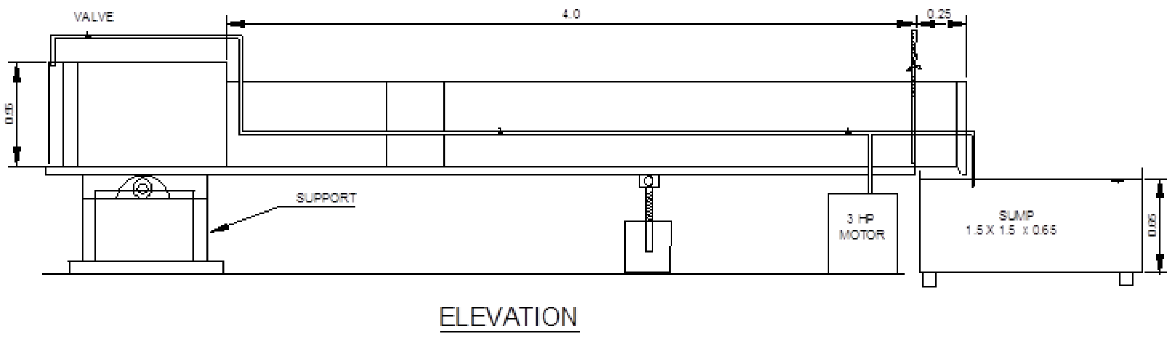

All dimensions are in meter

Figure 2 Experimental set up for computation of scour depth downstream of labyrinth weir

3. Observations and Discussion

As per the observations taken, the aspect ratio B/W as well as B/P are identified as important parameters which affect the scour depth downstream of labyrinth weir. The equations obtained by regression analysis are of power type with the following form (Figure 3 and Figure 4).

$$\frac{Z_m}{L} = k_1 \left(\frac{B}{W}\right)^{-n_1} \tag{1}$$

Where, the multiplier k_1 and n_1 depend on the length of apron provided downstream of the labyrinth weir .Following table 1 and table 2 given the values of k_1 and n_1.

Table 1 Range of discharge 0.01195 m^3/s to 0.01260 m^3/s

Extended apron Length	0 cm	5 cm	10 cm	15 cm
k_1	0.0565	0.0481	0.0434	0.0367
n_1	1.108	1.125	1.162	1.247
R^2	0.9268	0.9172	0.9285	0.9285

Table 2 Range of discharge 0.00765 m^3/s to 0.00988 m^3/s

Extended apron Length	0 cm	5 cm	10 cm	15 cm
k_1	0.0508	0.0414	0.0378	0.0304
n_1	1.138	1.266	1.267	1.441
R^2	0.9179	0.9243	0.9179	0.9529

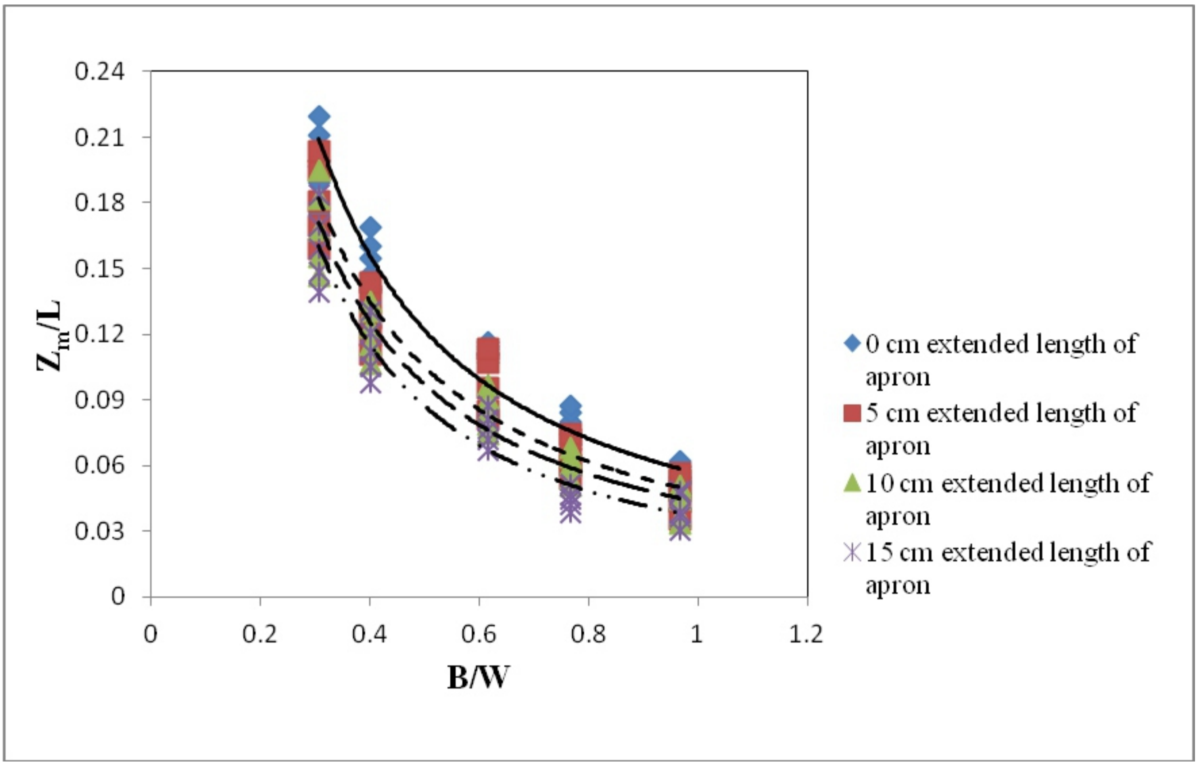

Figure 3 Variation of dimensionless maximum scour depth with aspect ratio (B/W)
[For side wall angle (α) ranging from 6^0- 21^0 and discharge (Q) ranging from 0.01195 m^3/s - 0.01260 m^3/s, t = 60s to t (max) = 3600s]

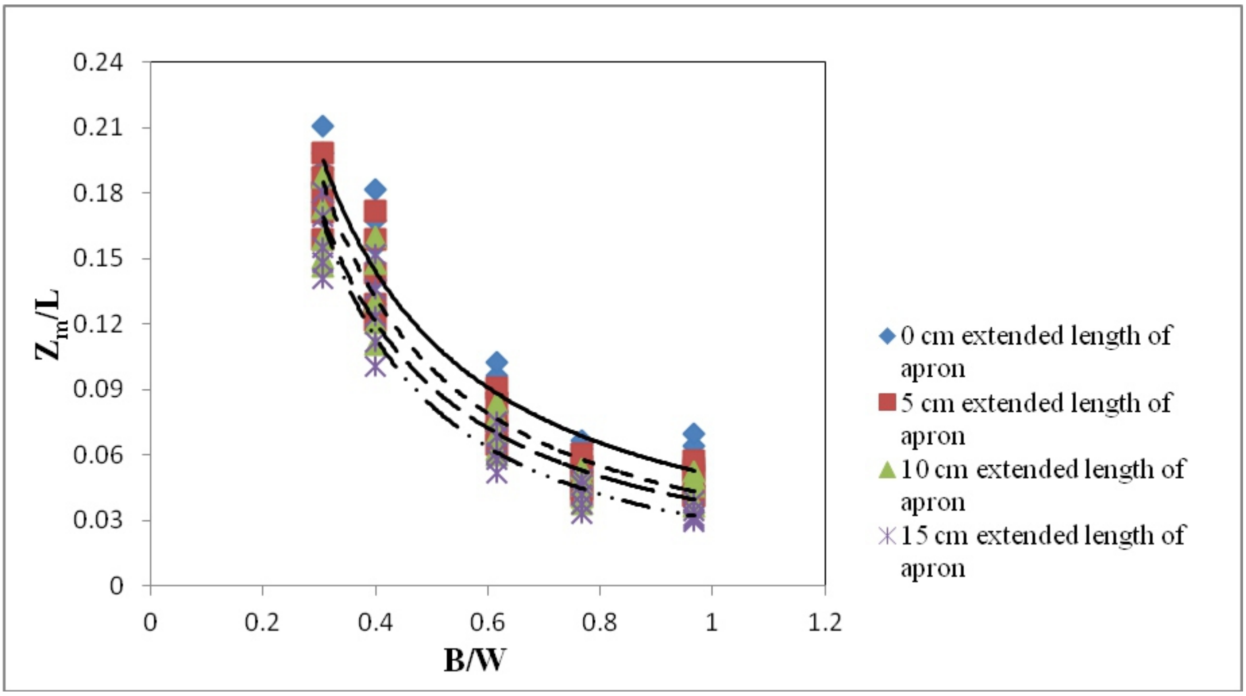

Figure 4 Variation of dimensionless maximum scour depth with aspect ratio (B/W)
[For side wall angle (α) ranging from 6^0- 21^0 and discharge (Q) ranging from 0.00765 m^3/s - 0.00988 m^3/s, t = 60s to t (max) = 3600s]

The aspect ratio B/P, where P is the height of labyrinth weir, yields the following results.

$$\frac{Z_m}{L} = k_2 \left(\frac{B}{P}\right)^{-n_2} \quad (2)$$

Where, the multiplier k_2 and n_2 follow the same pattern (Figure 5 and Figure 6) depending on the apron length provided. Following table 3 and table 4 given the values of k_2 and n_2.

Table 3 Range of discharge 0.01195 m^3/s to 0.01260 m^3/s

Extended apron Length	0 cm	5 cm	10 cm	15 cm
k_2	0.0601	0.0591	0.0536	0.0461
n_2	1.108	1.125	1.162	1.247
R^2	0.9268	0.9172	0.9368	0.9285

Table 4 Range of discharge 0.00765 m^3/s to 0.00988 m^3/s

Extended apron Length	0 cm	5 cm	10 cm	15 cm
k_2	0.0625	0.0522	0.0477	0.0396
n_2	1.138	1.266	1.267	1.441
R^2	0.9179	0.9243	0.9179	0.9529

It is interesting to note that though the values of k_1 and k_2 change in table 1 and table 3, values of n_1 and n_2 i.e. the exponent remain the same. The same can be stated for values of n_1 and n_2 in relation with table 2 table 4.

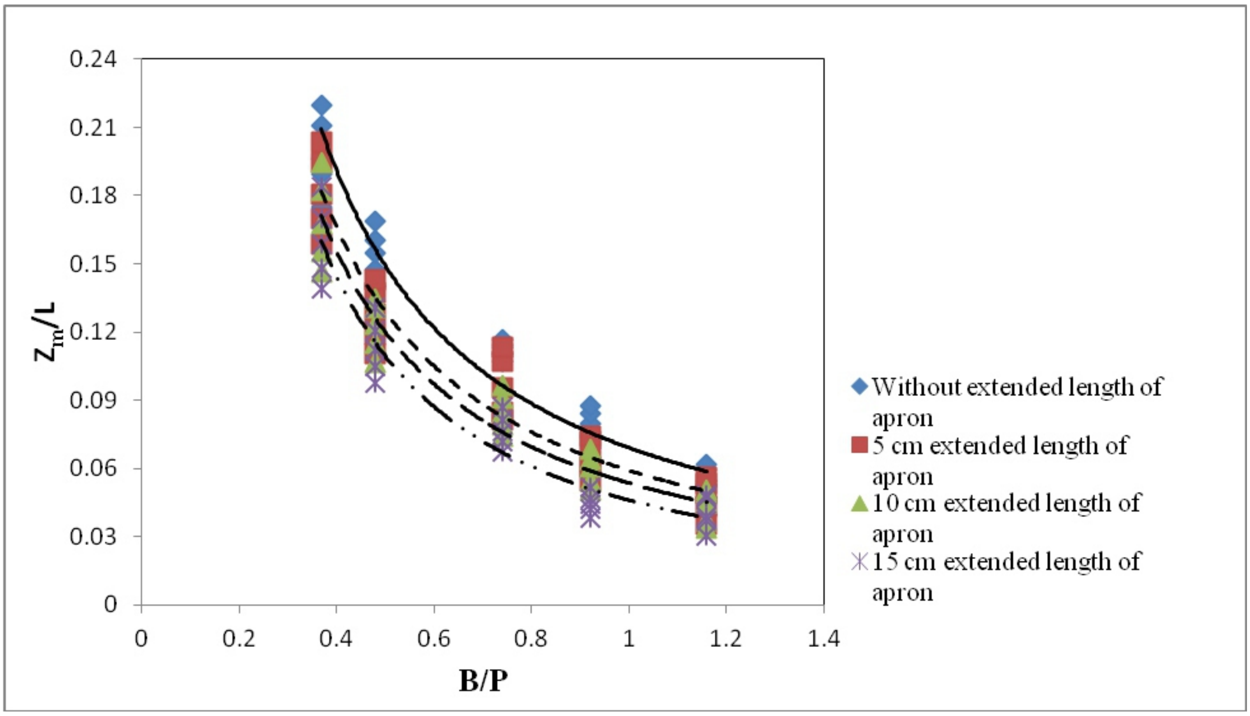

Figure 5 Variation of dimensionless maximum scour depth with aspect ratio (B/P)
[For side wall angle (α) ranging from 6^0 - 21^0 and discharge (Q) ranging from 0.01195 m^3/s - 0.01260 m^3/s, t = 60s to t (max) = 3600s]

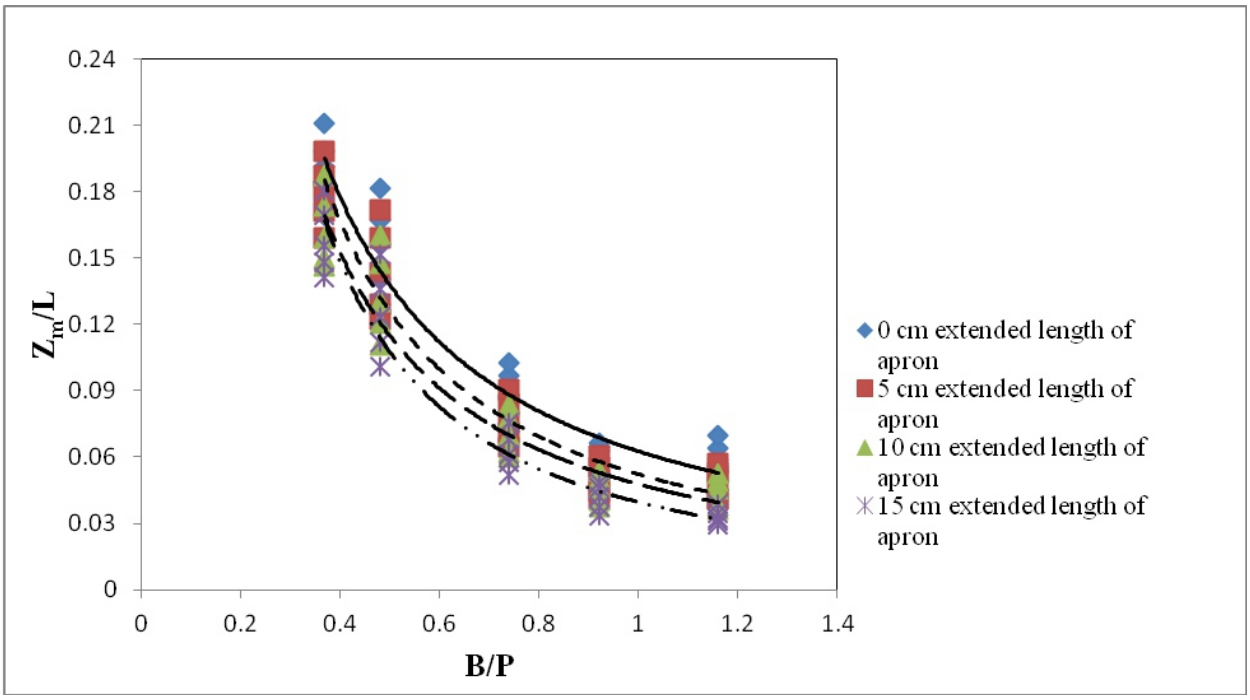

Figure 6 Variation of dimensionless maximum scour depth with aspect ratio (B/P)
[For side wall angle (α) ranging from 6^0 - 21^0 and discharge (Q) ranging from 0.00765 m/s^3 - 0.00988 m/s^3, t = 60s to t (max) = 3600s]

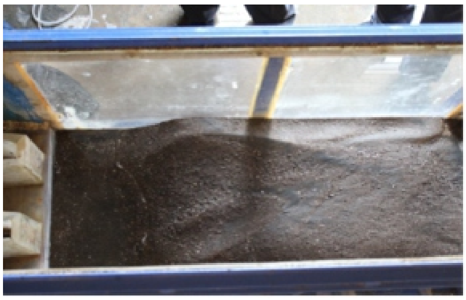

Figure 7 Scouring pattern for side wall angle (α) = 6^0, t(max) = 3600s with zero cm extended length of labyrinth apron.

Figure 8 Scouring pattern for side wall angle (α) = 6^0, t (max) = 3600s with 5 cm extended length of labyrinth apron

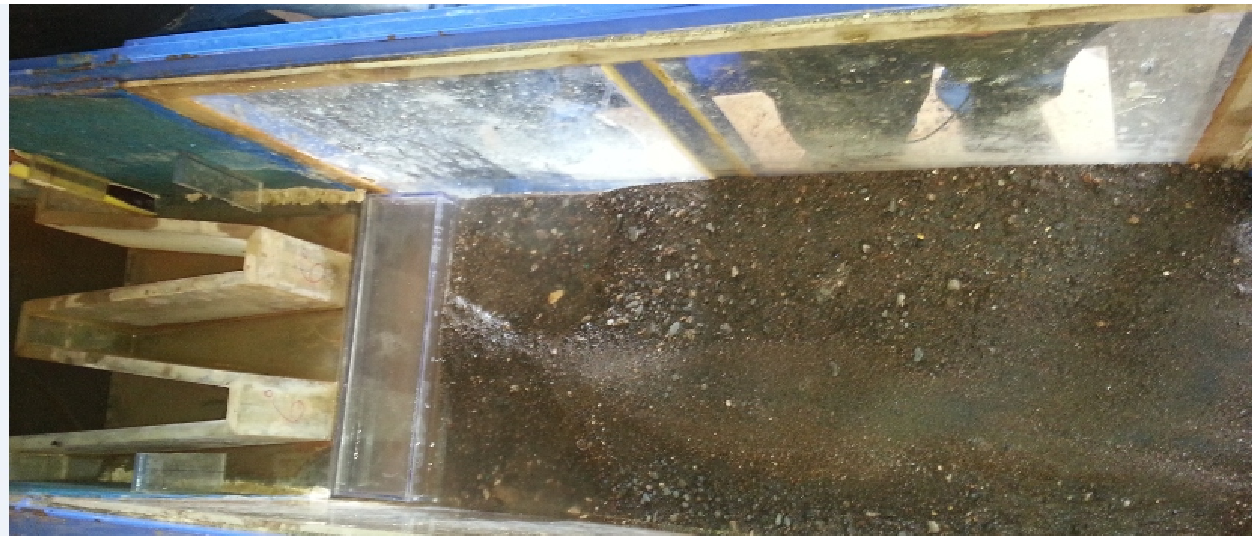

Figure 9 Scouring pattern for side wall angle (α) = 6^0, t (max) = 3600s with 10 cm extended length of labyrinth apron

Figure 10 Scouring pattern for side wall angle (α) = 6^0, t (max) = 3600s with 15 cm extended length of labyrinth apron

4. Conclusions

1. The aspect ratios B/W and B/P are identified as important parameters affecting the scour downstream of labyrinth weirs.
2. Providing apron of sufficient length is necessary in the design of labyrinth weir as the scour depth reduces if longer apron is provided.
3. A set of 16 equations of the basic form is developed which will be helpful in design of labyrinth weir.

$$\frac{Z_m}{L} = k_1\left(\frac{B}{W}\right)^{-n_1} \quad \text{and} \quad \frac{Z_m}{L} = k_2\left(\frac{B}{P}\right)^{-n_2}$$

4. It is observed that the scour depth decreases with the aspect ratios i.e. B/W and B/P.

5. Maximum scour depth is located just downstream of the labyrinth weir or end of apron if apron is provided. The scour pattern can be observed in the photographs.

Notation

L = Total length of labyrinth weir
W = Total width of labyrinth weir
w = Width of one cycle of labyrinth weir
B = Total length of labyrinth apron
D = Out-side apex width
A = Inside apex width
P = Height of labyrinth weir
α = Labyrinth side wall angle
Q = Discharge over labyrinth weir
Z_m= Maximum depth of scour
t = Time period
t (max) = Maximum time period

References

Bhuiyan, F., et al. (2007). "Hydraulic Evaluation of W-Weir for RiverRestoration." J. Hydraul. Eng., 10.1061/ (ASCE) 0733-9429(2007)133:6(596), 596–609.
Darvas, L. (1971). "Discussion of 'Performance and design of labyrinth weirs' by Hay and Taylor." J. Hydrol. Eng., 97(80), 1246–1251.
Falvey, H. (2003). Hydraulic design of labyrinth weirs, ASCE, Reston, VA.
Farhoudi, J. and K. Smith, 1985. Local Scour Profiles Downstream of Hydraulic Jump. Journal of Hydraulic Research, Vol. 23, No. 4, 343-359.
Gentiline, B.(1940) "stramazzi con cresta a plantaobliqua e a zig-zag." Memorie e studi dell instituto di idraulica e construzioni idraulich edel Regil politecnico di Milano, no.48 (In Italian).
Hamidifar, H., M.H. Omid, and M. Nasrabadi, 2011. Scour downstream of a rough rigid apron. World Applied Science Journal, (Accepted).
Hay, N., and Taylor, G. (1970). "Performance and design of labyrinth weirs." J. Hydraul. Eng., 96(11), 2337 2357
Hay, N., and Taylor, G. (1970). "Performance and design of labyrinth weirs." J. Hydrol. Eng., 96(11), 2337–2357
Khwairakpam, P., and A. Mazumdar, 2009. Local scour around hydraulic structures. International Journal of Recent Trends in Engineering, 1(6), 59-61.
Kotoulas, D. (1967) Das Kolkproblem unter besonderer Beriicksichtiguncj der Faktoren "Zeit" und "Geschiebemischung"im Rahmen der Wildbachverbauung.Schweizerische Anstalt fiir das Forstliche Versuchswesen, Vol 43, Heft 1.
Magalhães, A., and Lorena, M. (1989). "Hydraulic design of labyrinth weirs." Rep. No. 736, National Laboratory of Civil Engineering, Lisbon, Portugal.
Moghim, M. N., Dorsangi, M. G. and M. Ghodsian, 2008. Prediction of maximum scour depth due to wall jets by using neural networks, 4th National Congress on Civil Engineering, Tehran, Iran. (in Persian)
Pagliara, S. (2007), Influence of sediment gradation on scour downstream of block ramps, J. Hydraul. Eng. 133, 11, 1241-1248, DOI: 10.1061/(ASCE)0733- 9429(2007)133:11(1241).
Rosgen, D. L. _2001b_. "The cross vane, W-weir and J-hook structures: Their description, design and application for stream stabilization and river restoration." Proc., Wetland Engineering and River Restoration Conf. _CD-ROM_, ASCE, Reston, Va.
Shalash,M.S.E.(1959). Die Kolkbildung beim Ausfluss unter Schutzen. Diss. von der Fakultat fur Bauwesen der Techn. Hochschule Munchen.
Stefano Paglianra, MASCE (2014) "Scour of Clear Water Rock W-Weirs in Straight Rivers", Technical note, Journal of Hydraulic Engineering.
Tullis, P., Amanian, N., and Waldron, D. (1995). "Design of labyrinth weir spillways." J. Hydrol. Eng. 121(3), 247–255.

ISSN Application No. 21823

Experimental Investigation Of Wave Transformation Over A Sloping Bed

Srineash V K[1], Murali K [2]
[1]Research Scholar, Department of Ocean Engineering, IIT Madras, Chennai 600036, India.
[2]Proffesor, Department of Ocean Engineering, IIT Madras, Chennai 600036, India.
Email: srineash@gmail.com

A B S T R A C T

Ocean waves entering shallow waters from deep water region undergoes transformation. This study of wave transformation is very essential in predicting the behavior of waves on its propagation over the shallower region. As the wave enters shallow waters, there is a change in wave height due to shoaling effect. The study aims in comparing the theoretically established shoaling coefficient with the experimentally measured shoaling coefficient of the sloping bed. The results from the study will include the practical nonlinear effects along with the effect of steepness (gradient) of the sloping bed, which is not accounted by the shoaling coefficient calculated using linear wave theory. The hydrodynamic loading on structure gets altered with the variation of wave height. There may also be reflection from the sloping bed contributing to the increased wave height. Therefore the above factors contributing to the modification of wave height deems the necessity of having a sound understanding of the wave transformation phenomena. The present study will bring out the wave transformation over a given sloping bed. The variation of wave shoaling effect with respect to wave steepness and relative water depths will be presented along with the reflection characteristics of the sloping bottom. The results from the laboratory investigation performed in the shallow water wave flume of Department of Ocean Engineering, IIT Madras, will be presented.

Keywords: Shoaling, Wave steepness, Wave reflection, Sloping bottom.

1. Introduction

Ocean waves undergoes transformation on entering shallow waters from deep waters. The understanding of wave transformation is very essential to know about the coastal processes. The coastal structures present in the shallow waters are subjected to hydrodynamic loading in the form of waves. It is evident that the water depth decreases towards the shore. This decrease in water depth can be mimicked well in laboratory by using a sloping bed. As the wave enters shallow waters, there is an increase in wave height due to shoaling effect. Often there is a need to determine the incident wave height before the (structure to be studied) from the wave data measured offshore. The instantaneous wave elevations before the structure cannot be used to compute incident wave height as it includes the waves reflected from the structure. This knowledge of predicting the incident wave height from the deep water wave height is essential in order quantify the reflection, transmission and energy absorption characteristics of the coastal structure and also to determine the intensity of wave loading on the structure. Thus, this study focuses on the comparison of experimentally determined shoaling coefficient with the theoretical shoaling coefficient. The wave reflection characteristics of the submerged slopping bottom will also be brought out.

Nomenclature

H	Wave Height at 0.3 m water depth (m)
H_o	Wave Height at 0.67 m water depth (m)
T	Time period (s)
L	Wave length at 0.3 m water depth (m)
L_o	Deep water wavelength (m)
d	Water depth (m)
η	Wave Elevation (m)
K_r	Reflection coefficient
K_s	Shoaling coefficient
P_1	Wave Probe 1
P_2	Wave Probe 2
P_3	Wave Probe 3
ξ	Surf similarity parameter

2. Experimental Setup

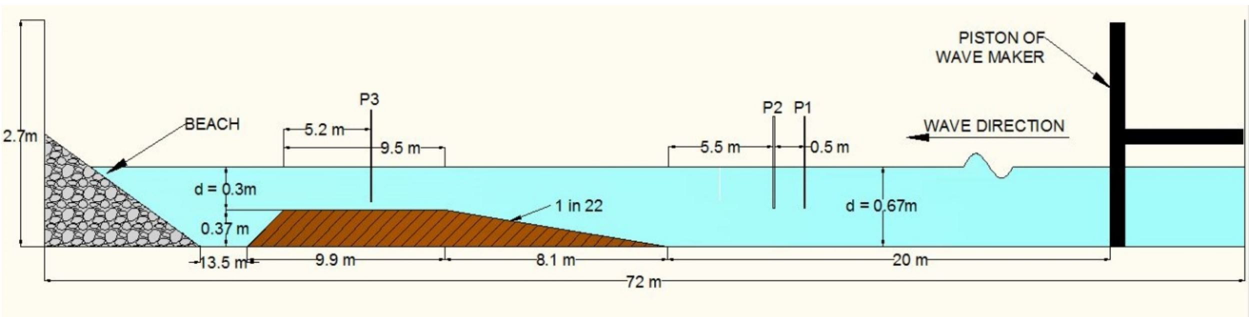

Figure 1 Schematic sketch of the experimental setup

The Laboratory was performed in the wave flume which is 72m long, 2m wide and 2.7 m deep. The submerged sloping bottom was provided with a slope of 1 in 22 to shoal the waves. Resistance type wave probes are used to find the instantaneous wave elevation. The data acquisition was done with a sampling frequency of 40 hertz. A Schematic sketch showing the experimental setup is shown in Fig. 1.

Two wave probes P1 and P2 was installed before the slopping bottom at a water depth of 0.67 m and wave probe P3 was installed at a water depth of 0.3 m after the slope. The probe P3 is used to measure the shoaled wave elevations and the probes P1 and P2 are used to find the instantaneous wave elevations of un-shoaled waves before the slope. The sloping bottom is provided at a distance of 20 from the wave paddle and the horizontal distance of the sloping bed is 8.1 m with a gradient of 1 in 22.

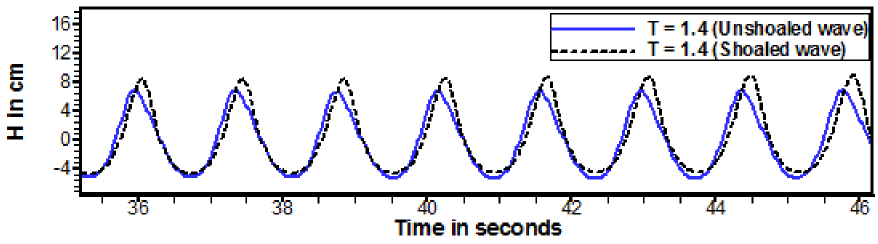

Figure 2 Typical time series for a d/L of 0.14

Figure 2 shows a typical time history of wave record corresponding to a d/L of 0.14 for a wave with a steepness as 0.065 at 0.67m water depth (for un-shoaled wave). In Fig. 2 the variation between shoaled wave past the submerged ramp and un-shoaled wave ahead of the submerged ramp is evident. This variation between the shoaled and un-shoaled wave will be studied in the further sections.

2.1 *Non-dimensional parameters used in study*

During the experiments, the relative water depth (d/L) was varied along with non-dimensional parameter H/d; where, the water depth was kept constant throughout the study. The reflection and shoaling coefficient examined in the study is found to depend on non-dimensional parameters as shown below.

$$(K_r, K_s) = f\,(d/L,\ H/L,\ H_o/L,\ H_o/L_o) \qquad (1)$$

The non-dimensional parameters and their ranges are shown in the table below.

Table 1 Range of non-dimensional parameters considered in study

Non dimensional parameters	Range
d/L	0.080 – 0.180
H/L	0.018- 0.055
H_o/L	0.018 – 0.060
H_o/L_o	0.012 – 0.040

3. Results and Discussions

The transformation of wave due to the shoaling process can be established with the theoretical shoaling coefficient. The theoretical shoaling coefficient is computed as discussed below.

$$K_s = \sqrt{\frac{n_1 \times c_1}{n_2 \times c_2}} \tag{2}$$

$$n = \frac{1}{2}\left[1 + \frac{4\pi d / L}{\sinh(4\pi d / L)}\right] \tag{3}$$

Where, K_s is the Shoaling coefficient.

C_1 corresponds to the celerity of wave in depths of 0.67 m and C_2 corresponds to the celerity of wave in depths of 0.3 m. n_1 corresponds to the value of n at 0.67m water depth and n_2 corresponds to values of n at 0.3m water depth.

3.1 *Influence of Wavelength on Shoaling coefficient*

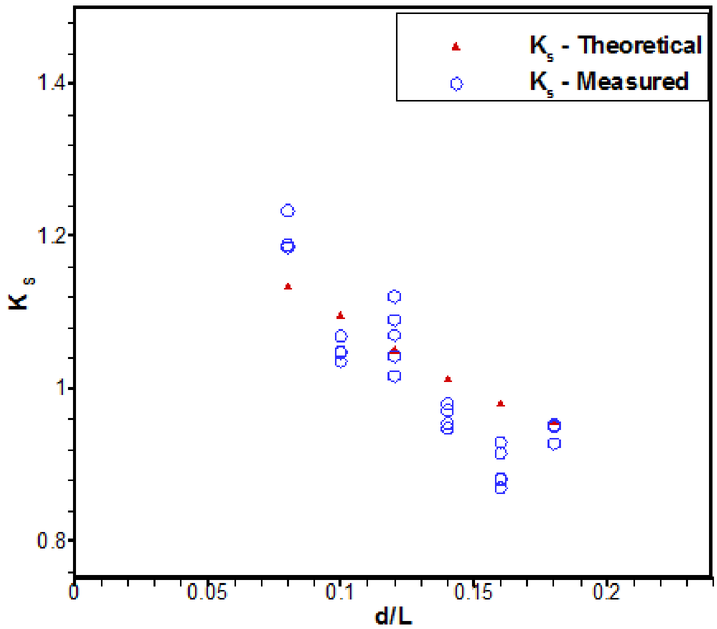

Figure 3 Variation of Ks with d/L

Figure 3 shows the variation of shoaling coefficient with relative water depth d/L. The shoaling coefficient increases with increase in wave length. In other words the shoaling coefficient increases with decrease in d/L. The effect of long wave is felt more in the bottom, and hence the sholing is found to be more dominating for a higher wavelength. From Fig. 3, it may be observed that the minimum theoretically computed shoaling coefficient is 0.95 for a d/L of 0.18 and a maximum shoaling coefficient of 1.13 is observed for a d/L of 0.08.

Further from Fig. 3 the experimentally measured shoaling coefficient is plotted along with the theoretically established shoaling coefficient. The experimentally measured shoaling coefficient is plotted against d/L. Variation of shoaling coefficient for given d/L was observed for different wave steepness H_0/L, which shows the effect of wave steepness on shoaling coefficient. However from Fig. 3 it may be inferred that the Wavelength plays in important role in shoaling effect than that of the wave steepness. The experimental shoaling coefficient follows a similar trend as that of the theoretical shoaling coefficient which increases with the increase in wavelength. It may be noted that the influence of wave steepness in experimentally measured shoaling coefficient is higher for higher wave length (lower d/L). For the experimentally measured shoaling coefficient, maximum shoaling coefficient was found to be 1.23 for a d/L of 0.08. The minimum measured shoaling coefficient was found to be 0.87 for a d/L of 0.16.

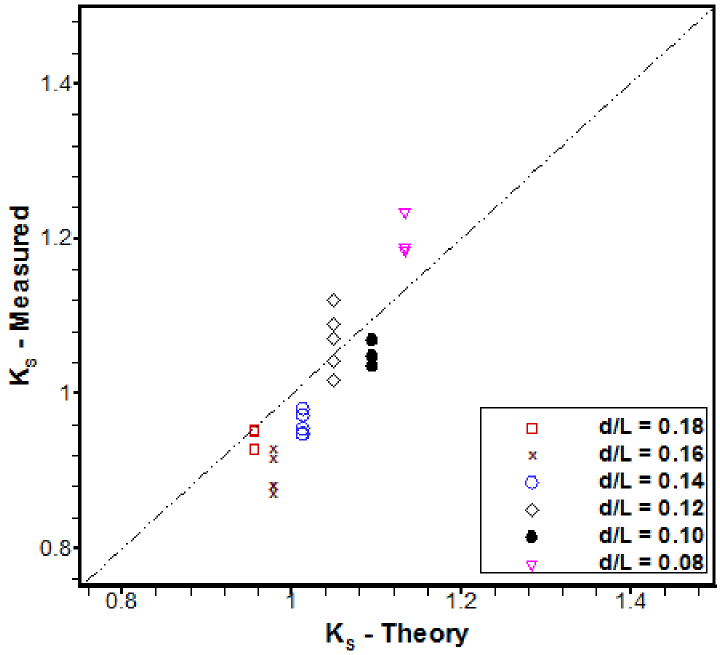

Figure 4 Comparison of $K_s^{(THEORY)}$ With $K_s^{(MEASURED)}$

Figure 4 shows the comparison of shoaling coefficient obtained by theoretical computation with that of the experimentally measured shoaling coefficient. From the plot it can be observed that within the given range of d/L the theory compares well with the measured values. Further the variation of shoaling coefficient with change in wave steepness is observed in experiment which is not accounted in theory.

3.2 *Effect of Wavelength on Wave Reflection*

Ocean waves gets reflected on facing obstruction. In the present study the wave reflection of a submerged slope is studied. The reflection analysis is performed based on two probe approach (Goda et al., 1976) and the wave probes P1 and P2 were used to find the reflection coefficient of the slopping bed.

To understand the process of wave reflection better, the test results of reflection coefficients are plotted as a function of wave steepness against the relative water depth d/L. From Fig. 5 it may be interpreted that the increase in wave length increases the wave reflection. This may be because the effect of wave on the sloping bottom is more for a longer wave and hence higher reflection is noticed for a long wave. The maximum wave reflection found was about 0.15 for a d/L of 0.08. The minimum reflection value noticed is 0.046 for a d/L of 0.18.

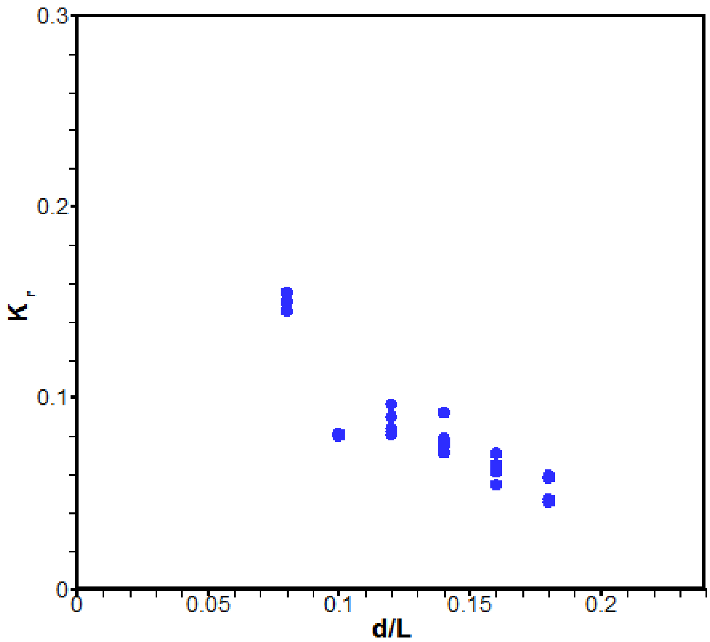

Figure 5 Variation of Kr with d/L

3.3 *Role of Surf Similarity Parameter*

Surf similarity parameter is an important parameter to describe the coastal process as the parameter takes into account of the gradient of the bottom slope. The surf similarity parameter is calculated as shown below.

Surf similarity parameter, $\xi = \frac{tan\theta}{\sqrt{\frac{H_o}{L_o}}}$ (4)

Where,

tanθ takes into account of the bottom gradient. The value fed to the tanθ is constant throughout the study and it is 1 by 22. It has to be noted that the surf similarity parameter is a single parameter accounting the steepness of the wave and the gradient of the sloping bed. In the present study efforts are taken to find the influence of sloping bed and the wave steepness on the phenomena of wave transformation.

The shoaling coefficient is plotted against surf similarity parameter in Fig. 6 and it can be noticed that for a higher d/L values (lower wavelength), the Shoaling coefficient K_s is found to be low, whereas for lower d/L values (longer wavelength), the shoaling is observed to be higher. There is an increasing trend of shoaling observed with the increase in surf similarity parameter. For Higher wavelength a drastic raise in shoaling is observed. It may be interpreted from Fig. 6 that the effect of steepness of wave and the gradient of bottom slope plays a role in wave transformation. There is significant increase in shoaling observed for d/L greater than 0.1. From the Fig. 6 the maximum shoaling coefficient is found to be 1.19 for a d/L of 0.08 with a value of surf similarity parameter about 0.39. The minimum value of shoaling coefficient was found to be about 0.87 for a d/L of 0.16 with a surf similarity parameter as 0.33.

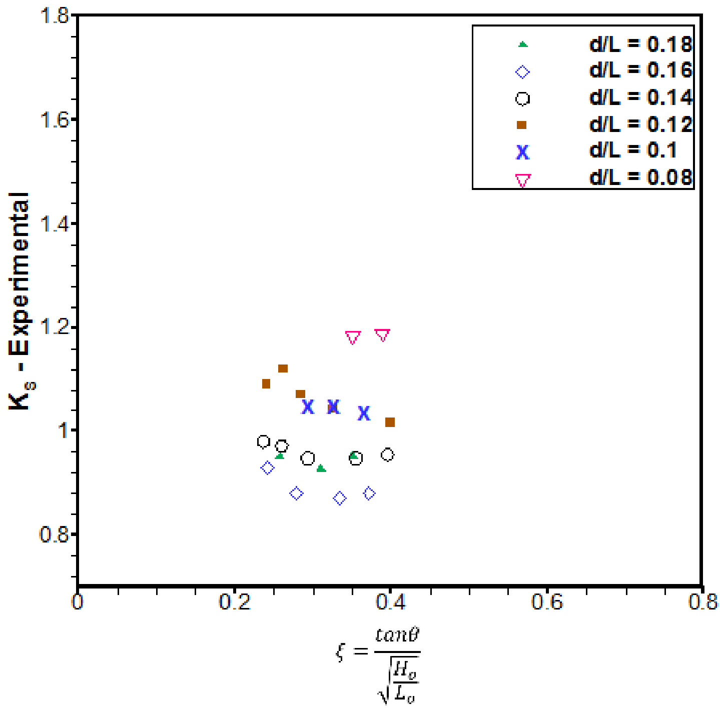

Figure 6 Variation of K_s with surf similarity parameter

4. Conclusions

The Theoretical shoaling coefficient (K_s) is a function of wavelength and independent of wave height. During the experiments, slight variation of shoaling coefficient was found due to the effect of wave heights. The dependability of shoaling coefficient with wave height is found and plotted in the study. Further, the theoretically computed shoaling coefficient was compared with the experimentally measured shoaling coefficient.

The slope of the bottom ramp is not accounted in the theory. The present study takes into account of the slope of bottom which is presented using surf similarity parameter.

For studies on coastal structures, which deems the necessity of knowledge of incident wave height from the deep water wave record; present study gives a much realistic measure of wave shoaling based on experimental results.

The reflection effect due to the bottom sloping bed was plotted with respect to the wavelength and quantified.

References

Allsop. N.W.H., Durand. N., and Hurdle. D. P., (1998). Influence of steep seabed slopes on breaking waves for Structure design. Journal of Coastal Engineering, 906 – 919.

Ching-Piao, Tsai., Hong-Bin, Chen., John R,-C, Hsu., (2001). Calculations of wave transformation across the surf zone. Journal of Ocean Engineering, (28) 941–955.

Ching-Piao, Tsai., Hong-Bin, Hwung-Hweng Hwung., Ming-Jen, Huang., (2005). Examination of empirical formulas for wave shoaling and breaking on steep slopes. Journal of Ocean Engineering, (32) 469-483.

Dean, R. G., and Dalrymple. R. A., (1984). Water Wave Mechanicsfor Engineers and Scientists Prentice-Halll, Englewood Cliffs, New Jersey.

Goda, Y., and Suzuki, Y., (1976). Estimation of Incident and Reflected Waves in Random wave Experiments. Proceedings of 15th Coastal Engineering Conference, (1), 828-845.

Srineash, V. K., and Murali, K., (2015). Hydrodynamic performance of Gabion Box Artificial Reefs. Proceedings of the Twenty-fifth International Ocean and Polar Engineering Conference
Kona, Big Island, Hawaii, USA.

Shore Protection Manual (1984). Coastal Engineering Research Centre, US Army Corps of Engineers. Volume 1, chapter 2, 122 – 124.

Ice Thickness Estimation Using Geospatial Technology

Sanjay Manohar Bisht, Praveen Kumar Thakur, Arpit Chouksey, Shiv Prasad Agarwal
Water Resources Department,
Indian Institute of Remote Sensing, 4-Kalidas Road, Dehradun-248001, India
Email: praveen@iirs.gov.in

ABSTRACT

The present study estimates ice thickness distribution over the Gangotri group of glaciers using modelling techniques. The modelling techniques follows the flow law of ice and empirical relation between the slope and height relation found for glacier system over the world. Surface velocity was calculated using multi-temporal PAN data from Landsat 7/8 (15m) and Indian Remote Sensing Satellite IRS-1C/1D (5m) data over the years 1998 to 2014. This study uses for the first time IRS-1C/1D for Gangotri glacier velocity estimation. Sub-pixel correlation of the images were done using COSI-Corr software. The study was able to successfully conclude the measured velocity to that of 0.02m/day for the duration of 1998-2014 over the whole glacier. Velocity over accumulation zone was found to be 0.041m/day. Also the modelled ice depth was analyzed and found to be in range of 58 to 450 m for the entire glacier. Few small area in middle and upper part of glacier showed values between 450-650m. The ice depth found at snout varied from 58 m to 67 m. Finally the modelled depth was correlated to the Terrestrial Laser Scanner (TLS) field measurements and was found to be in having a correlation of R2=0.799. The estimated ice depth matches well with earlier reported studies for Gangotri glacier.

Keywords:Glacier Velocity, Landsat, IRS 1C/1D, Ice flow model, Glacier Depth, TLS, Glacier dynamics

1. Introduction

The Himalayan–Karakoram (HK) region has the largest glacier coverage outside the Polar Regions but knowledge of the dimensions of these glaciers and their behavior in response to climate change is still limited, due to their remoteness, the harsh topography, the complex political situation, and the associated difficult physical access (Bolch et al., 2012). Glaciers influence the runoff regime of major river systems affecting millions of people down river (Immerzeel et al., 2010; Kaser et al., 2010). Of these glaciers, the Gangotri group of glacier is a prominent system of glaciers as it is the first source of water in the Ganga Basin affecting large part of north India. Furthermore, applications of modern methodologies, such as measurements of gravity field anomalies (Jacob et al., 2012) or laser altimetry (Kääb et al., 2012), and combinations of them with field data (Gardner et al., 2013) lead to deviating findings, underlining the difficulty of measuring complex processes in such a large region.Two of the major parameters used to characterize glacier dynamics are surface velocity and ice thickness

(Gantayat et al., 2014). In this work, therefore, we estimate the ice thickness distribution over Gangotri Glacier. The surface velocities were estimated using feature tracking based techniques using medium to high resolution ortho-rectified and co-registered remote-sensing data (Leprince et al., 2007). Here, we also focus on determining the ice depth for the Gangotri group of glacier, which is a basic parameter required for glacier melt projections (Huss et al., 2008; Gabbi et al., 2012), and estimates of future sea-level rise contributions due to glacier melt.

To estimate glacier volumes various methods have been proposed over time, such as volume–area (V–A) relations (e.g., Chen and Ohmura, 1990; Bahr et al., 1997), slope-dependent ice thickness estimations (Haeberli and Hoelzle, 1995), and more recently spatially distributed ice-thickness models (Linsbauer et al., 2009; Cuffey and Patterson, 2010; Huss and Farinotti, 2012; Li et al., 2012; Clarke et al. 2013). Power-law relationships for volume/area, volume/length and volume/area/length have been derived from the abundant information available regarding area and length (Chen and Ohmura, 1990; Bahr et al., 1997; Radić et al., 2010). First estimate of the ice thickness distribution of all glaciers around the globe was presented by Huss and Farinotti (2012). Artificial neural network methods have also been employed, using calculations based on a digital elevation model (DEM) and a mask of present-day ice cover in the Mount Waddington area in British Columbia and Yukon, Canada (Clarke and others, 2009). These networks are trained by substituting the known topography of ice-free regions, adjacent to the ice-covered regions of interest in case of non-availability of data providing maximum relative uncertainty in volume estimates at 45%. Ice volume was calculated for Columbia Glacier, Alaska, USA, by estimating ice fluxes using the equation of continuity between adjacent flowlines (McNabb and others, 2012).

In that investigation surface velocities and mass balance were used to estimate mean ice flux. Farinotti and others (2009a) developed another approach, using apparent mass balance to estimate ice thickness. From a distribution of apparent mass balance, ice flux was computed over selected ice flowlines and was then converted to ice thickness using Glen's flow law (Glen, 1955). Using this method, the ice-thickness distribution and volumes were estimated for glaciers in the Swiss Alps and elsewhere (Farinotti and others, 2009b; Huss and Farinotti, 2012). Mass-balance distribution data over large glaciers in the Himalaya are not easily available and are inaccurate in some cases (Bolch et. al.,2012).

Here, we present ice volume estimations for the Gangotri group of glacier using three different V–A relations, a slope-dependent ice thickness estimation method, an ice-thickness distribution model and a model using surface velocities, slope and the flow law of ice. These methods are applied to the same base data, comprising the 90 m digital elevation model (DEM) from the Shuttle Radar Topography

Mission (SRTM). Results from the different approaches are then correlated at snout using the Terrestrial laser Scanner (TLS) based ground survey during 15-17 Sep. 2014.

1.1 Study region and data

The study area consists of the Gangotri group of glacier in the Gharwal Himalayas of India. The Gangotri glacier is one of the largest glaciers in the Himalayas, being approximately 30 km long with a width varying between 0.5 and 2.5 km. It has a height varying between 4000 and 7000 m.a.s.l. (Jain, S.K., 2008). The Gangotri glacier is a valley type glacier, flowing into the NW direction. Of the Gangotri glacier, approximately 29% of the total area is affected by debris. The three main tributaries are Raktvarn (15.90 km), Chaturangi (22.45 km) and Kirti (11.05 km) (Figure 1) and five other tributaries contribute to the Gangotri glacier. The present land forms are the result of erosion and deposition processes of glacial-periglacial features.

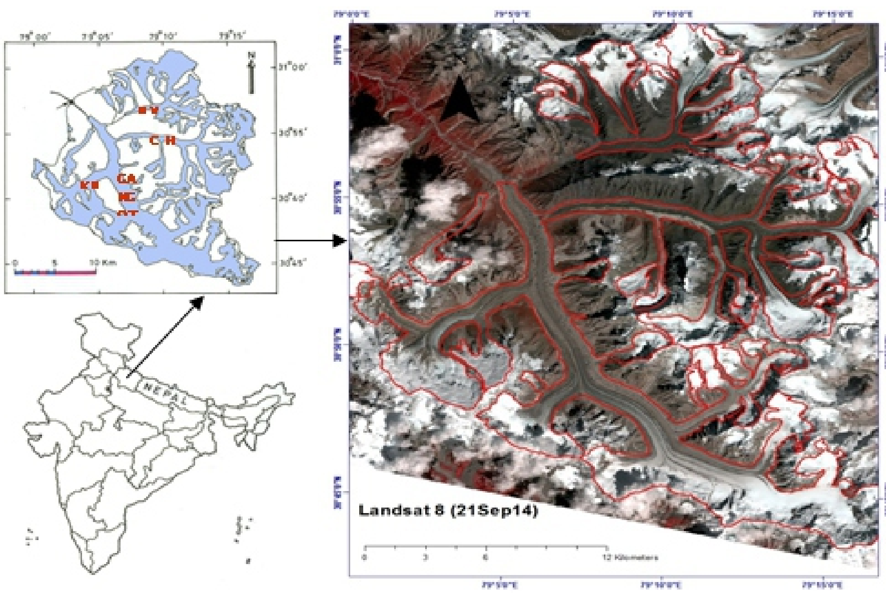

Figure Location map and FCC image ofGangotri Group of Glacier

2. Experimental program

In the following section, the different ice volume estimation approaches applied in this study are described. Methodologies description are restricted to short summaries and background information can be studied from the given reference of the study.

2.1 Area-related thickness estimations

The most frequently used approach for ice volume estimations so far is V–A scaling method. As large glaciers generally tend to be thicker ice volume is calculated as a function of its surface area. Area-related scaling techniques have been extensively applied as their application is simple, fast and area data had been measured and compiled long before digital terrain information became available, hence a long term data is available. V–A scaling relation is generally represented as:

$V = cA^{\gamma}$ (1)

Where, V represents the glacier volume, A the glacier area, γ and c are two scaling parameters.

In order to facilitate comparisons with results from other methods and ice thickness measurements, Eq. (1) can be translated into the thickness–area relation as:

$H = cA^{B}$

Where, H represents the ice thickness and $\beta = \gamma$-1.

Here we use three sets of scaling parameters, applied in (Frey et al., 2014): (i) Chen and Ohmura (1990), (ii) Bahr et al. (1997), and (iii) LIGG et al. (1988). These parameters have been applied for the whole H-K range but a local study is the parameters and its accuracy is tested.The applied scaling parameters used in this study are given in Table 1.

Table 1. Parameter of the applied V-A relations

Extended apron Length	0 cm	5 cm	10 cm	15 cm
k_2	0.0625	0.0522	0.0477	0.0396
n_2	1.138	1.266	1.267	1.441
R^2	0.9179	0.9243	0.9179	0.9529

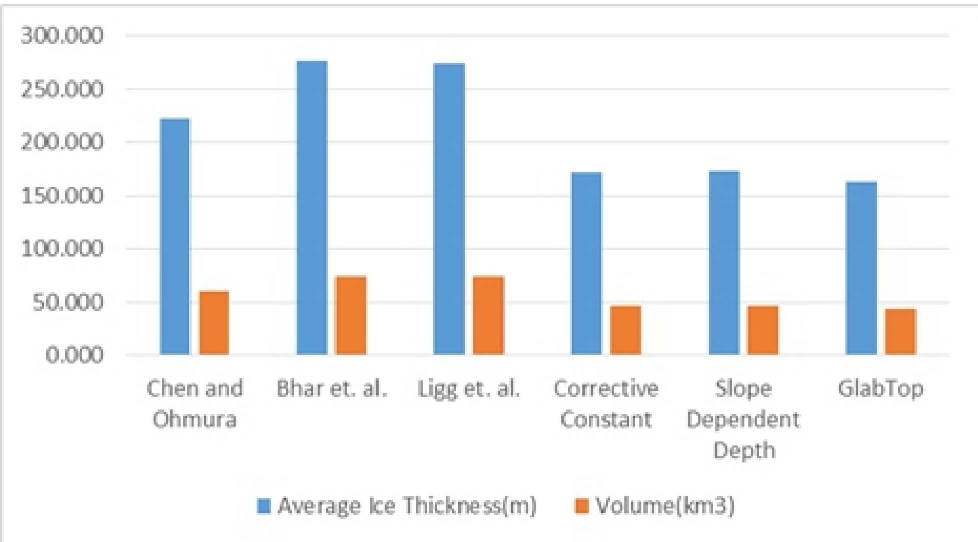

Figure 2 Comparative listing of results of the Study Note: Axis-y the in figure represents numerical value for both average ice thickness (denoted by m) and average total volume calculated from the relation (denoted by km^3).

A comparative list of the methods employed for ice depth is shown in Figure 2. As is clearly seen in the graph both GlabTop and slope dependent method are nearer to each other as expected. But other models using the old V-A (Volume-Area) scaling technique are constantly overestimating the mean glacier depth. When compared to velocity dependent Laminar flow based model, the mean depth drops to more than 20m at 92m. Hence a corrective constant for Gangotri Glacier is suggested which are more in line to the results from other models. New factors based on studying the depth in this study are suggested for Gangotri group of glaciers for further V-A analysis in future is suggested as c = 0.193 and γ = 1.35.

2.2*Slope-dependent thickness estimations and GlabTop*

Haeberli and Hoelzle(1995) presented a way to estimate glacier volume using average surface slope and vertical glacier relief. This parameterization scheme has been used over Himalayan range in recent studies (Frey et al., 2014). Therefore, an application of this approach can be used for depth estimation over the study area.Here the equation governing the depth at center flow line of the glacier can be written as:

$$h_{centre} = \frac{\tau}{f\sigma g sin\alpha} \quad (3)$$

The shape factor, f, is determined from (Cuffey and Paterson, 2010)

Table.2 Shape Factor for different glacier geometries

W		F	
	Parabola	Semi-ellipse	Rectangle
1	0.445	0.5	0.558
2	0.646	0.709	0.789
3	0.746	0.799	0.884
4	0.806	0.849	
∞	1	1	1

Which is typically chose at 0.8 for valley glaciers. To interpolate the value at centre flow line over the whole of glacier taking the edges of the glacier to be at 0 ice depth, a multiplication of π/4 is applied.

$$h_G = h_{centre}\left(\frac{\pi}{4}\right) \quad (4)$$

The change in basal stress in accordance with elevation range is based on reconstructed late Pleistocene glaciers of European Alps (Paul and Linsbauer, 2012). Where,

$$\tau = \begin{cases} 0.5 + 159.81\mathrm{H} - 43.5(\Delta H)^2, & \Delta H \leq 1.6km \\ 150, & \Delta H > 1.6km \end{cases} \quad (5)$$

When applied over remotely sensed data, these parameters need to be considered for accurate determination. Hence ΔH (difference in height from snout to peak of glacier involved) and glacier length l is used to determine slope of the glacier using the equation:

$$\alpha_l = arctan\left(\frac{\Delta H}{l}\right) \tag{6}$$

This is then used to calculate the stress for the main glacier branch and consecutively centre flow line depth. This flow line depth is then interpolated to the glacier boundary which is fixed at zero depth using equation (4).

Paul and Linsbauer (2012)used an hybrid approach using inputs fromClarke et al., (2009) and Li et al., (2011), which considers just the flow dynamics and enables the bed estimation to be computationally very fast. The GlabTop model approach uses hydrological correct approach of digitizing flow-lines and takes into consideration the changes in τ every 500m, whereas slope dependant model does not consider variable τ but takes mean value for full glacier.

The DEM used for the study is converted into a contour line with 50 m elevation difference. This is then converted into slope map and equation (5) is applied to calculate the value of τ. This is then used to calculate the ice depth distribution along the flow lines which are digitized earlier following the contour lines. The TopoToRaster tool is used from the ArcGIS to interpolate the values of the ice depth over the entire glacier from the flow line to the entire glacier.

2.3*Ice Thickness from velocity measurement*

2.3.1 *Velocity Measurement*

Surface velocities of the glacier were calculated using sub-pixel correlation of the acquired multi temporal images, using the ENVI module Co-registration of Optically Sensed Images and Correlation (COSI-Corr), which is downloadable at http:// www.tectonics.caltech.edu/. The algorithm uses two images to iteratively cross-correlate in the phase plane on sliding windows, to find the best possible correlation. A detailed description of the algorithm is given by (Leprince et al., 2007). The setup provides alteration of the window size, window movement, signal to noise ratio threshold and gridded output options. The setting of these depend on the expected movement of the glacier and the pixel resolution of the image. Table 2. Provides us with the setting used in the velocities measurements. All pixels that have SNR < 0.9 and displacements >85m are discarded. A vector field is generated from the two displacement images and is then overlaid on the image to check the accuracy of the measurement. The difference in the time of acquisition between the two images is used to estimate the velocity field.

$$D_{s=\sqrt{(E-S^2)+(N-S^2)}} \quad (7)$$

Where, D_s represent the translation movement detected, E-S represent the movement values for the E-S direction and N-S represent the movement values for the N-S direction. Although care has to be taken to disregard all pixel having SNR less than 0.9, hence leaving patches of area with no movement values. This is then rectified by interpolating nearby values. Velocity calculation is then a simple matter of movement divided by the time interval between the two scenes. This is done using vector addition of the two fields of movement with the angle between them always at 90. This is used to get the magnitude of the movement of the feature over the search window. Also local averaging is done to filter out rouge pixel showing movement values very high which are obviously termed as noise.

Table 3 COSI-Corr Settings used in the study

Window Size		Resolution (m)	Step	Robustness Iteration	Mask Threshold
Initial	Final				
64	32	15	2	4	0.9
128	64	15	2	4	0.9
256	64	5	2	4	0.9
256	128	5	2	4	0.9
512	256	5	2	4	0.9

2.3.2 *Estimation of Depth*

Ice thickness calculation are done using velocity values derived from the COSI-CORR software. The basic premise behind the model for thickness estimation follows the logic of Basal Shear stress and Velocities in "Laminar flow" as described in (Cuffey and Patterson, 2010). Here the model of a glacier is a parallel-sided slab of ice of thickness H on a rough plane of slope α. No sliding of the slab is assumed on the plane and the thickness of the slab is much less than its length and width. The slab is perpendicular to the plane and of unit cross section. The weight of the slab is ρgH. Where ρ is density of ice, g is acceleration due to gravity and H is the height of the slab. The weight of the slab along the surface will be countered by basal stress which will be equal to:

$$\tau_b = \rho g H sin\alpha \quad (8)$$

This is a very simple model for glacier movement when the layers of ice do not move over each other. But in real world scenarios, ice moves over each layer and hence velocity varies with depth. This is shown in Figure 1. Here a block of ice is taken with unit length at all sides. This give rise to the premise that these blocks of ice move over each other hence producing sliding motion.

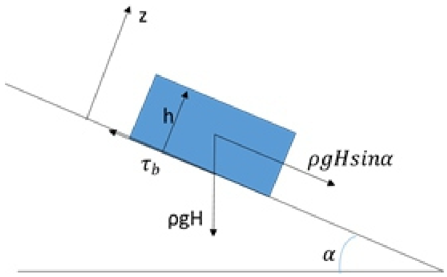

Figure 3 Forces acting on a block of ice

Let u be the x component of the velocity. Assuming the slab deforms in a simple shear, the flow lines are parallel to surface. This is Laminar flow of ice. It follows that the z component of the velocity is zero and so shear strain rate is ½(du/dz).

$$\frac{1}{2}\frac{du}{dz} = A\tau_b^n \qquad (9)$$

Where, A is a creep parameter (which depends on temperature,fabric, grain size and impurity content and has a value of$3.24*10^{24}$ Pa^{-3} s^{-1} for temperate glaciers (Cuffey and Paterson, 2010).Using equation (8) and adding a scale/shape factor, f, for temperate glaciers we get

$$\tau_b = f\rho g(h-z)sin\alpha \qquad (10)$$

Integrating equation (9) into (8) we get

$$u_s - u(z) = \frac{2A}{n+1}(f\rho gsin\alpha)^n(h-z)^{n+1} \quad \alpha \qquad (11)$$

This equation can then be used to determine the depth/height of the ice over any glacier where our assumption holds true. Changing the equation into the final form by replacing (h-z) with H we get.

$$u_s - u_b = \frac{2A}{n+1}(f\rho gsin\alpha)^n(H)^{n+1} \qquad (12)$$

Rearranging to get depth information of a particular velocity pair, we get:

$$H = \sqrt[n+1]{\frac{(n+1)(u_s-u_b)}{2A(f\rho gsin\alpha)^n}} \qquad (13)$$

Where, f is a scale factor, i.e. the ratiobetween the driving stress and basal stress along a glacier, and has a range of [0.8, 1] for temperate glaciers. This study has used f = 0.8 (Haeberli and Hoelzle, 1995), ρ is the ice density, assigned a constant value of 900 kgm^{-3} (Farinotti and others, 2009a), g is accelerationdue to gravity ($9.8ms^{-2}$) and Slope,α is estimated from 90 m SRTM-DEM.

3. Results and uncertainty analysis

Table 4 and Table 5 provide the results derived from slope dependent model and GlabTop respectively.

These approaches work on the same premise as explained in Section 2.

Table 4 Slope Dependent Model Parameters and Results

Name	Length (km)	ΔH(km)	Slope (rad)	τ	Ice depth (m)	Area Covered (km^2)
Gangotri	30	3.2	0.10626	150	200.42	87.87
Raktvarn	10.27	2	0.19233	150	111.21	47.88
Chaturangi	15.18	1.2	0.07888	129.62	233.1	64.89
Swachand	6.81	1.15	0.16729	126.7413	107.87	16.11
Malandi	4.26	0.85	0.19694	104.9013	75.97	4.58
Meru	8.53	1.45	0.16837	140.7513	119.03	5.57
Kirti	9.01	2	0.21843	150	98.1	31.6
Ghanohim	4.03	0.6	0.14779	80.72	77.68	11.83

The Ice depth is the most in the main trunk and Chaturangi glacier at 222.10m and 233.10m respectively. These are also some of the largest spanning glaciers in the group. This supports the hypothesis that states the depth as directly proportional to its area. All other glacier branches are medium in depth (75.97m to 119.03m) with the average depth and volume calculated to be 172.88m and 46.7376km^3 for the whole glacier.

Table 5 Slope Dependent Model Parameters and Results

Name	Length (km)	ΔH (km)	α(rad)	τ	Ice depth (m)	Area Covered (km^2)
Gangotri	30	3.2	0.10626	150	200.42	68.4
Raktvarn	10.27	2	0.19233	150	111.21	47.88
Swachand	15.18	1.2	0.07888	129.62	233.1	64.89
Swachand	6.81	1.15	0.16729	126.7413	107.87	16.11
Malandi	4.26	0.85	0.19694	104.9013	75.97	4.58
Meru	8.53	1.45	0.16837	140.7513	119.03	5.57
Kirti	9.01	2	0.21843	150	98.1	31.6
Ghanohim	4.03	0.6	0.14779	80.72	77.68	11.83
Gangotri2	4.7	1	0.20963	116.8	79.54	19.47

GlabTop model (Paul and Linsbauer, 2012) uses the same technique as defined for slope dependent approach but depth calculation are done for height intervals. This means that the branch lines digitized are more intensive and conform to the hydrological structure of the glacier bed. Hence τ, basal sheer stress, is calculated for height interval of 500m each. This allows for more flexibility in calculating ice depth or bed topography of complex glacier system like Gangotri.

Table 6 provide velocity measurement from the COSI-Corr parameterization used in the Table 3 for all the image pairs used in the study. This includes both medium and high resolution images.

Table 6 Velocity measurement from COSI-Corr for related image pairs

Satellite	Date Pair	Window Size Initial	Window Size Final	Resolution (m)	Movement E-W	Movement N-S	SNR	Time Interval	Velocity (m/day)
Landsat 7	9Sep98-22Oct99	64	32	15	9.974	6.22	0.9	408	0.0288
Landsat 7	8Oct00-20Oct01	64	32	15	8.89	6.812	0.9	377	0.0297
Landsat 7	22Oct99-8Oct00	64	32	15	4.893	3.59	0.9	352	0.0172
Landsat 7	20Oct01-8Jun02	64	32	15	6.172	7.04	0.9	231	0.0405
Landsat 7	22Oct99-20Oct01	128	64	15	14.183	10.188	0.9	729	0.0239
Landsat 7	8Oct00-28Aug02	128	64	15	8.511	10.638	0.9	689	0.0197
Landsat 7	9Sep98-8Oct00	128	64	15	10.389	8.46	0.9	760	0.0176
Landsat 8	26Aug13-21Sep14	64	32	15	5.396	6.509	0.9	391	0.0216
IRS	22Oct00-08Jul02	256	64	5	6.889	7.323	0.9	624	0.0161
IRS	22Oct00-05Oct03	256	64	5	7.554	8.215	0.9	1078	0.0103
IRS	8Jul02-20Oct05	256	64	5	5.968	5.609	0.9	1200	0.0068
IRS	8Jul02-5Oct03	128	32	5	7.902	7.281	0.9	454	0.0236
IRS	5Oct03-20Oct05	256	64	5	5.553	5.491	0.9	746	0.0104

The average velocity for the period of observation from 9 September 1998 to 21 September 2014 was calculated to be 0.02 m day $^{-1}$for whole glacier. This observation when limited to upper areas of the observation yielded an average movement of 0.041 m day $^{-1}$.This observation when limited to upper areas of the observation yielded an average movement of 0.041 m day-1. Velocity from earlier reported papers varies from 0.038–0.233 m day–1 in the accumulation region to 0.055–0.0821 m day–1 near the snout (Gantayat et al., 2014). Kumar et. al., (2008) reported Gangotri glacier retreat using rapid static and kinematic GPS survey to be in range of 0.033-0.0376 mday-1 (during 2004-2005). Saraswat et al. (2013) showed that Gangotri glacier snout has receded at a rate of 21.3 ± 3 myear−1 (0.058 mday-1) over a period of 6 years (2004–2010). Further, the average glacier surface velocity in the northern (lower) portions (28.1 ± 2.3 m year−1 or 0.077 mday-1) is observed to be significantly lower than in the southern (higher) portions (48.1 ± 2.3 m year−1 or 0.13 mday-1) of the Gangotri glacier.

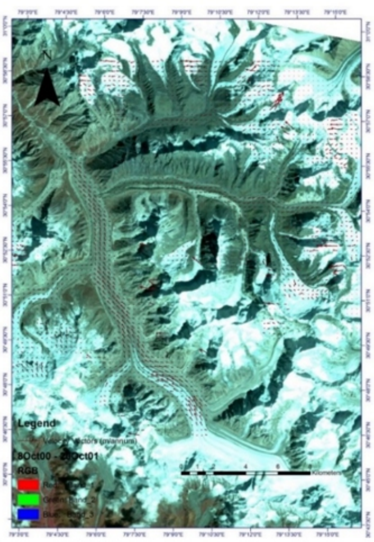

Figure 4 Velocity Vectors over Gangotri Glacier

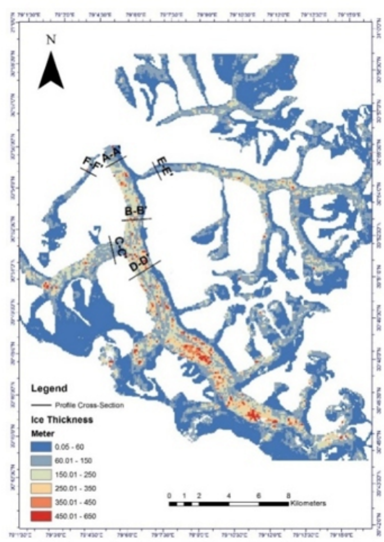

Figure 5 Mean Ice Depth Profile of Gangotri Glacier from time of analysis (1998-2014).

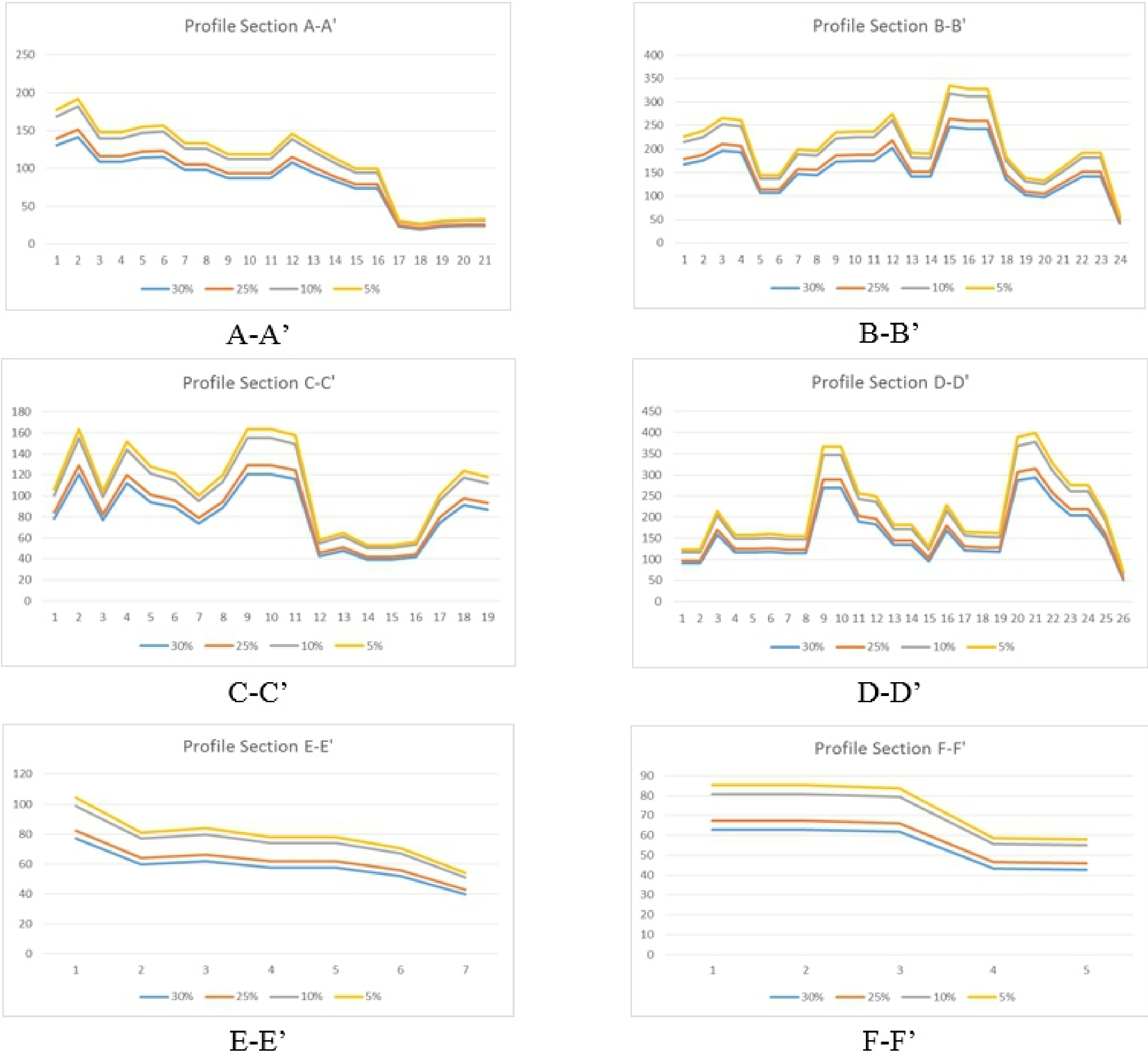

Figure 6 Profile cross-Section for different ratio of basal velocity(in terms of percentage of surface velocity) Note: (A-F) x-axis represent the profile length (100m interval) from x-x'; y-axis represents ice thickness calculated from the model.

The major conclusion of the profile analysis have shown that the variation in Lamiar flow model is very huge where variation from 20m to 400m is easily visible. Also the depth at snout was found to be ~60 m and the maximum depth was found at accuumulation zone at ~650 m.

Uncertainty analysis procedure wassimilar to as reported in (Gantayat et al., 2014). In present study, velocity uncertaintyon snow free ground for IRS 1C/1D is in range of 0 to 0.351 m and a maximum of 1.5 m. Values for uncertainty of surface velocity was fixed at 3.5 m annum^{-1}based on observed values by (Swaroop et. al., 2003). Scaling factor uncertainty was set at 0.1 (Gantayat et al., 2014). Creep factor uncertainty was set at $8.24*10^{25}$ (Farinotti et al., 2009a). Uncertainty over ice density accuracy is taken at 90 kgm^{-3} i.e. 10% of the defined density used in the study. Uncertainty in the slope estimation using SRTM DEM is calculated to be at 0.001. All the reported uncertainty are then added for uncertainty in the volume estimation of the Glacier which is reported to be 11.4% for the current study. A marked decrease of uncertainty by 7% from earlier reported study (Gantayat*et. al.,* 2014). This is possible due to use of high resolution imagery (5 to 15m as compared to 30 m) (Farinotti*et. al.,* 2009) used for velocity estimation and better vertical relative accuracy achieved from STRM DEM (± 10 m) as compared to ASTER GDEM(± 20 m).

4 Validation and discussions

Ice thickness was validated by TLS measurement at snout for 9 Points. These were kept at a distance of 30 m to 100 m apart from each other. The scan of the area was taken and overlaid over the model output. This is then used to measure the thickness of the ice from a stone visible in the scan and detached from the main glacier, lying in the river bed. This stone was used as reference for the thickness measurement which varied from 58 m to 67 m at snout validating the model estimation of ice thickness at ~60 m.Gantayat*et. al.,* (2014) reported the maximum ice thickness as 540 m to 50–60 m as minimum at snout. This is slightly different from present study, where minimum ice thickness at snout is estimated as 60 – 67 m and 650 m as maximum ice thickness. This difference can be attributed to different data source with high resolution data such as IRS 1C/1D Pan Data and 90 m SRTM DEM based slope.

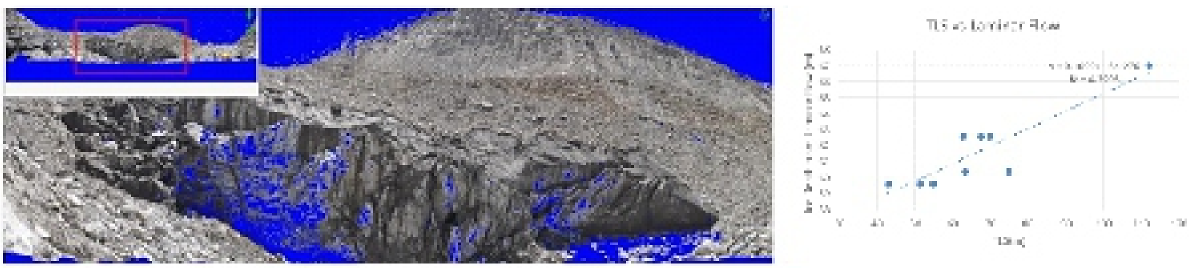

Figure 7 Correlation between TLS ground Measurements and Laminar Flow Model at snout and the Actual Scan of the snout during field visit (15-17 September 2014)

Frey et al., 2014 has reported an average ice depth as 145 m for GlabTop2 Model and 91 m for Slopedependent thickness estimate. The study concludes the average thickness of the Gangotri Glacier to be 92.25 m which is close to the reported value by (Frey et al., 2014). Future work can include use of Ground Penetrating Radar (GPR) for depth measurement and validation of the ice thickness for whole glacier. Field survey using DGPS can be done to validate surface velocity of the glacier. Parameterization of the laminar flow model for density, scaling factor, creep factor, and basal velocity can be further studied for better results.

Acknowledgement:

Authors express their sincere thanks to Director IIRS, A Senthil Kumar and former Director YVN Krishnamurthy for their constant support encouragement and all institutional facilities to complete this work. Thanks are also due for Head and faculty of Photogrammetry and Remote Sensing Department (PRSD) for providing and training of TLS and DGPS operations used in field survey, CMD IIRS and VSSC Trivandrum Engineers to provide solar panels and fuel cell based instrument charging systems, Forest Department Uttarakhand and SASE Chandigarh for giving permission to visit Gangotri glacier and stay at Bhojbasa, NRSC Data Centre (NDC) and USGS for providing satellite data used in this study.

References

Bahr, D. B., Meier, M. F., and Peckham, S. D.: The physical basisof glacier volume–area scaling, J. Geophys. Res.-Solid, 102,20355–20362, 1997.

Bolch, T., Kulkarni, A., Kääb, A., Huggel, C., Paul, F., Cogley, J.G., Frey, H., Kargel, J. S., Fujita, K., Scheel, M., Bajracharya,S., and Stoffel, M.: The State and Fate of Himalayan Glaciers,Science, 336, 310–314, doi:10.1126/science.1215828, 2012.

Chen, J. and Ohmura, A.: Estimation of Alpine glacier water resourcesand their change since the 1870s, IAHS Publications –Hydrology in Mountainous Regions, I – Hydrological Measurements;the water cycle, Proceedings of two Lausanne Symposia,August 1990, edited by: Lang, H. and Musy, A., IAHS Publ.,193, 127–135, 1990.

Clarke, G., Anslow, F., Jarosch, A., Radic, V., Menounos, B., Bolch, T., and Berthier, E.: Ice volume and subglacial topography for western Canadian glaciers from mass balance fields, thinning rates, and a bed stress model. J. Climate, 26, 4282–4303, doi:10.1175/JCLI-D-12-00513.1, 2013.

Cuffey, K.M., Paterson, W.S.B., 2010. The Physics of Glaciers. Elsevier Science.

Farinotti, D. and Huss, M.: An upper-bound estimate for the accuracy of glacier volume–area scaling, The Cryosphere, 7, 1707– 1720, doi: 10.5194/tc-7-1707-2013, 2013.

Farinotti, D., Huss, M., Bauder, A., Funk, M., and Truffer, M.: A method to estimate the ice volume and ice-thickness distribution of alpine glaciers, J. Glaciol., 55, 422–430, 2009.

Farinotti D, Huss M, Bauder A, Funk M and Truffer M. A method to estimate ice volume and ice-thickness distribution of alpine glaciers. J. Glaciol., 55(191), 422–430, doi: 10.3189/ 002214309788816759, 2009a.

Farinotti D, Huss M, Bauder A and Funk M. An estimate of the glacier ice volume in the Swiss Alps. Global Planet. Change, 68(3), 225–231, doi: 10.1016/j.gloplacha.2009.05.004, 2009b.

Frey, H., Machguth, H., Huss, M., Huggel, C., Bajracharya, S., Bolch, T., Kulkarni, A., Linsbauer, A., Salzmann, N., Stoffel, M. Estimating the volume of glaciers in the Himalayan-Karakoram region using different methods. The Cryosphere 8, 2313–2333. doi:10.5194/tc-8-2313-2014, 2014

Gabbi, J., Farinotti, D., Bauder, A., and Maurer, H.: Ice volume distribution and implications on runoff projections in a glacierized catchment, Hydrol. Earth Syst. Sci., 16, 4543–4556, doi: 10.5194/hess-16-4543-2012, 2012.

Gantayat, P., Kulkarni, A. V., and Srinivasan, J., Estimation of ice thickness using surface velocities and slope: case study at Gangotri Glacier, India, Journal Of Glaciology, Vol. 60, No. 220, doi: 10.3189/2014JoG13J078, 2014.

Gardner, A. S., Moholdt, G., Cogley, J. G., Wouters, B., Arendt, A. A., Wahr, J., Berthier, E., Hock, R., Pfeffer, W. T., Kaser, G., Ligtenberg, S. R. M., Bolch, T., Sharp, M. J., Hagen, J. O., Van den Broeke, M. R., and Paul, F.: A Reconciled Estimate of Glacier Contributions to Sea Level Rise: 2003 to 2009, Science, 340, 852–857, doi:10.1126/science.1234532, 2013.

Glen, J. W.: The Creep of Polycrystalline Ice, P. Roy. Soc. A, 228, 519–538, doi:10.1098/rspa.1955.0066, 1955.

Haeberli,W. and Hoelzle, M.: Application of inventory data for estimating characteristics of and regional climate-change effects on mountain glaciers: a pilot study with the European Alps, Ann. Glaciol., 21, 206–212, 1995.
Huss, M. and Farinotti, D.: Distributed ice thickness and volume of all glaciers around the globe, J. Geophys. Res., 117, F04010, doi: 10.1029/2012JF002523, 2012.
Huss, M., Farinotti, D., and Bauder, A.: Modelling runoff from highly glacierized alpine drainage basins in a changing climate, Hydrol. Process. 22, 3888–3902, doi:10.1002/hyp.7055, 2008.
Immerzeel, W. W., van Beek, L. P. H., and Bierkens, M. F. P.: Climate Change Will Affect the Asian Water Towers, Science, 328, 1382–1385, doi:10.1126/science.1183188, 2010.
Jacob, T., Wahr, J., Pfeffer, W. T., and Swenson, S.: Recent contributions of glaciers and ice caps to sea level rise, Nature, 482, 514–518, doi:10.1038/nature10847, 2012.
Jain SK (2008) Impact of retreat of Gangotri glacier on the flow of Ganga River. Current Sci., 95(8), 1012–1014
Kääb, A., Berthier, E., Nuth, C., Gardelle, J., and Arnaud, Y.: Contrasting patterns of early twenty-first-century glacier mass change in the Himalayas, Nature, 488, 495–498, doi: 10.1038/nature11324, 2012.
Kamb, B. and Echelmeyer, K.: Stress-gradient coupling in glacier flow, I: Longitudinal averaging of the influence of ice thickness and surface slope, J. Glaciol., 32, 267–284, 1986.
Kaser, G., Grosshauser, M., and Marzeion, B.: Contribution potential of glaciers to water availability in different climate regimes, P. Natl. Acad. Sci. USA, 107, 20233–20227, doi:10.1073/pnas.1008162107, 2010.
Leprince S, Barbot S, Ayoub F and Avouac J-P (2007) Automatic and precise orthorectification, coregistration, and subpixel correlation of satellite images, application to ground deformation measurements. IEEE Trans. Geosci. Remote Sens., 45(6), 1529– 1558 (doi: 10.1109/TGRS.2006.888937).
Li, H., Ng, F., Li, Z., Qin, D., and Cheng, G.: An extended "perfect-plasticity" method for estimating ice thickness along the flow line of mountain glaciers, J. Geophys. Res., 117, F01020, doi: 10.1029/2011JF002104, 2011.
Linsbauer, A., Paul, F., Hoelzle, M., Frey, H., and Haeberli, W.: The Swiss Alps without Glaciers – A GIS-based Modelling Approach for Reconstruction of Glacier Beds, in: Proceedings of Geomorphometry 2009, edited by: Purves, R., Gruber, S., Straumann, R., and Hengl, T., University of Zurich, Zurich, 243–247, 2009.
LIGG, WECS, and NEA: Report on first expedition to glaciers and glacier lakes in the Pumqu (Arun) and Poiqu (Bhote-Sun Kosi) river basins, Xizang (Tibet), China, Science Press, Beijing, China, 1988.
McNabb, R. W., Hock, R., O'Neel, S., Rasmussen, L. A., Ahn, Y., Braun, M., Conway, H., Herreid, S., Joughin, I., Pfeffer, W. T., Smith, B. E., and Truffer, M.: Using surface velocities to calculate ice thickness and bed topography: a case study at Columbia Glacier, Alaska, USA, J. Glaciol., 58, 1151–1164, 2012.
Frey, H., Machguth, H., Huss, M., Huggel, C., Bajracharya, S., Bolch, T., Kulkarni, A., Linsbauer, A., Salzmann, N., Stoffel, M., 2014. Estimating the volume of glaciers in the Himalayan–Karakoram region using different methods. The Cryosphere 8, 2313–2333. doi:10.5194/tc-8-2313-2014
Paul, F., Linsbauer, A., 2012. Modeling of glacier bed topography from glacier outlines, central branch lines, and a DEM. Int. J. Geogr. Inf. Sci. 26, 1173–1190. doi:10.1080/13658816.2011.627859
Radi´c, V. and Hock, R.: Regional and global volumes of glaciers derived from statistical upscaling of glacier inventory data, J. Geophys. Res., 115, F01010, doi:10.1029/2009JF001373, 2010.
Saraswat, P., Syed,T.H., Famiglietti, J.S., Fielding, E.J., Crippen, R. Gupta, N. Recent changes in the snout position and surface velocity of 592 Gangotri glacier observed from space. International Journal of Remote Sensing, 34:24, 8653-8668, doi: 10.1080/01431161.2013.845923, 2013.
Swaroop S, Raina VK and Sangeswar CV (2003) Ice flow of Gangotri glacier. In Srivastava D, Gupta KR and Mukerji S eds. Proceedings of the Workshop on Gangotri glacier, 26–28 March 2003, Lucknow, India. (Spec. Publ. 80) Geological Survey of India, Kolkataata

ISSN Application No. 21823

Prevention Of Scour Around Bridge Abutments Using Inclined Plates

Upain Kumar Bhatia[1], Baldev Setia [2]

[1] Associate Professor in Civil Engineering, Maharishi Markandeshwar Engineering College Mullana, India.

[2] Professor, Department of Civil Engineering, National Institute of Technology, Kurukshetra, India.

Email: upainbhatia@mmumullana.org

ABSTRACT

Bridge failures due to hydraulic conditions and their protection against scour had been a subject area in various domains. The present paper is the outcome of an experimental study, which in turn is a part of bigger and more comprehensive investigation on scour around abutments. Presented work emphasizes the prevention of local scour around short vertical wall abutment models using thin plates attached inclined to their upstream face. Flow visualization study has also been carried out to ascertain the favorable flow modification by the proposed scour prevention device. Three dye-based techniques named dye injection, dye diffusion and sticky dye diffusion techniques have been employed for this purpose. The device was found to offer a solid inclined barrier to the oncoming flow, and promising to be effective scour prevention as well as scour protection device. Authors have also attempted and presented three dimensional visualization of the flow by using stereoscopy.

Scour studies involved 5-hours experimental runs conducted under incipient flow condition with fine sediment (d_{50}= 0.28mm) in a 15m long, 0.6m wide and 0.75m deep re-circulating flume. The height and angle of inclination of the inclined plate were varied to arrive at the optimum configuration, which has been found to offer protection against scour of about 70%.

Keywords: Scour, Abutment, Visualization, scour protection

1. Introduction

An inclined plate is a thin plate installed at an inclination to the upstream face of a short vertical wall abutment model and sufficiently embedded into the sediment bed. It principally possesses the flow altering capabilities by generating vortices opposite to the horse shoe vortex. Figure 1 presents schematic of the geometrical arrangement of an inclined plate on the upstream front of a short vertical wall abutment. Height of inclined plate above the sediment bed (z) and its Angle of inclination (α) are the geometrical parameters affecting its performance.

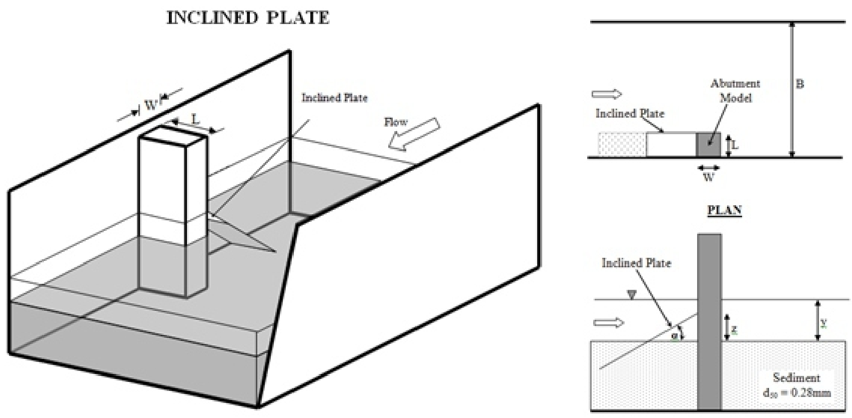

L = Protruding length of abutment
W = Width of abutment
B = Width of flume
y = Flow depth
Y_{sm} = Maximum scour depth around abutment
d_{50} = Median size of sediment
v = Approach velocity
z = Elevation of top edge of inclined plate above the bed
α = Angle of inclination of inclined plate with horizontal

2. Concept and Mechanism of Flow Modification

An inclined plate offers protection against abutment scour by offering a solid barrier or shield against the oncoming flow. This shield being inclined offers a ramp to deflect the bottom layers and generates secondary vortices opposite to the scour-causing principal vortex. In addition to the above, it also causes shifting of the point of scour initiation away from the upstream corner of the abutment.

A Perspex model of short vertical wall abutment (L = W = 33mm) installed with an inclined plate (Figure 2a) was tested for flow visualization studies using dye injection, dye diffusion and sticky dye diffusion techniques. Potassium Permanganate was used as dye. Steady uniform flow conditions were maintained at a Reynolds Number of 860.

The dye injected above the inclined plate was observed to be rising up the inclined ramp and deflecting towards the channel and turning into secondary vortices in the zone of constriction (Figure 2b). The direction of these vortices in this zone is opposite to the direction of scour-causing principal vortex. Figures 2(c and d) present, in plan and oblique view respectively, the photographic visualization of flow confined within the triangular wedge shaped space under the inclined plate. The water in this portion appears to rotate slowly with centre at the circular spot of dye near the abutment. A thin streak of dye was observed to be emanating upward from this centre and gently moving out to the mainstream.

The flow pattern in the bottom layers in the channel was visualized around the assembly using dye diffusion technique. The flow streaks in the constriction zone, near the abutment-device assembly (Figure 2e) are indicative of the direction of flow lines towards the abutment. Further, deposition of dye within the triangular wedge shaped space below the inclined plate indicates the deadness of water in that region. It is a manifestation of the scour protection capability of the device. Figure 2(f) shows the dye streaks emanating from the inclined plate using sticky dye diffusion technique. The dye streaks are clearly turning and generating secondary vortices in the zone of constriction.

The flow modification as shown in Figures 2(c and d) has also been illustrated in Figure 3 as a pair of stereo images ***Left*** and ***Right***. These images can be visualized in 3D form by parallel eyed viewing or through a stereoscope.

3. Effect of Height of Inclined Plate above the Sediment Bed

An inclined plate of width equal to protruding length (L) of abutment was installed at six different vertical locations 0.0L, 0.5L, 1.0L, 1.5L, 2.0L and 2.5L above the bed. Details of test conditions and the maximum scour depths obtained have been shown in Table 1.

Figure 4 presents the effect of height of inclined plate on non-dimensionalized maximum scour depth (Y_{sm}/ L) of abutment and Figure 5 presents the performance potential of all the configurations tested in this set of experiments.

The inclined plates tested in this series were found capable of providing scour reduction ranging from 43.03% for z = 0.0L (i.e. at bed level) to 70.80% for z = 1.0L above the bed. A closer look at the results also indicates that there is not much difference in the performance potentials for the different elevations of the inclined plate above the average bed. All values are marginally differing and fall within a band of 10% variation. For the case when the top of the plate coincides with the average bed level the scour depth is high (0.8L) and the corresponding performance potential is only 43%. However, viewed from the aspect of ease of construction and cost effectiveness, the inclined plate may be safely placed with its top edge at bed level or at an elevation equal to half the length of abutment above the average bed level.

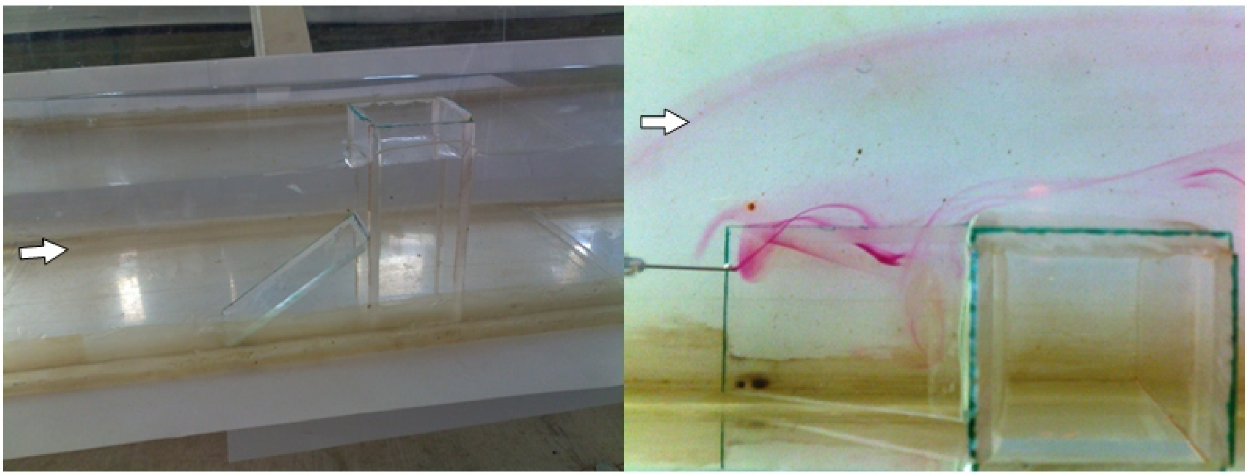

(a)
Abutment with inclined plate placed in flume

(b)
Dye being released above the inclined plate
Secondary circulations are visible

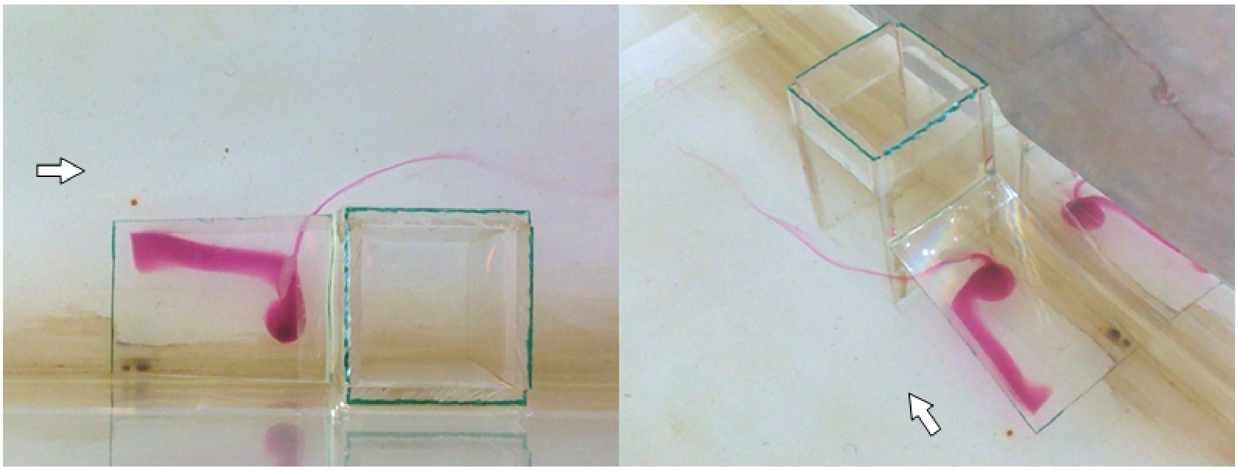

(c)
Flow modification below the inclined plate

(d)
Oblique view of the flow below inclined plate

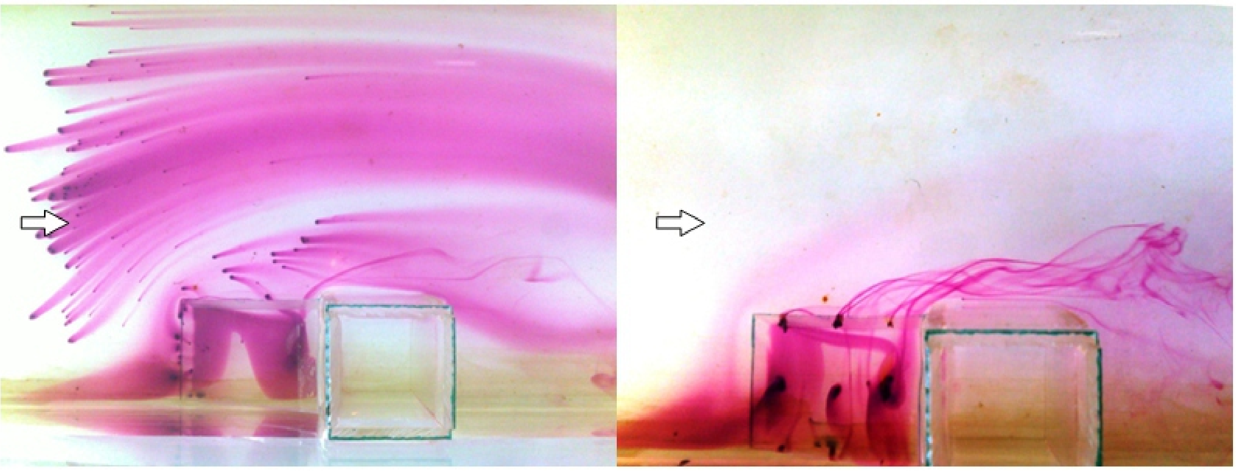

(e)
Flow around assembly (dye diffusion technique)

(f)
flow above the inclined (sticky dye diffusion technique). Secondary vortices are visible.

Figure 2: Photographic Views of Flow Modification due to an Inclined Plate
(Dye: $KMnO_4$ Re= 840)

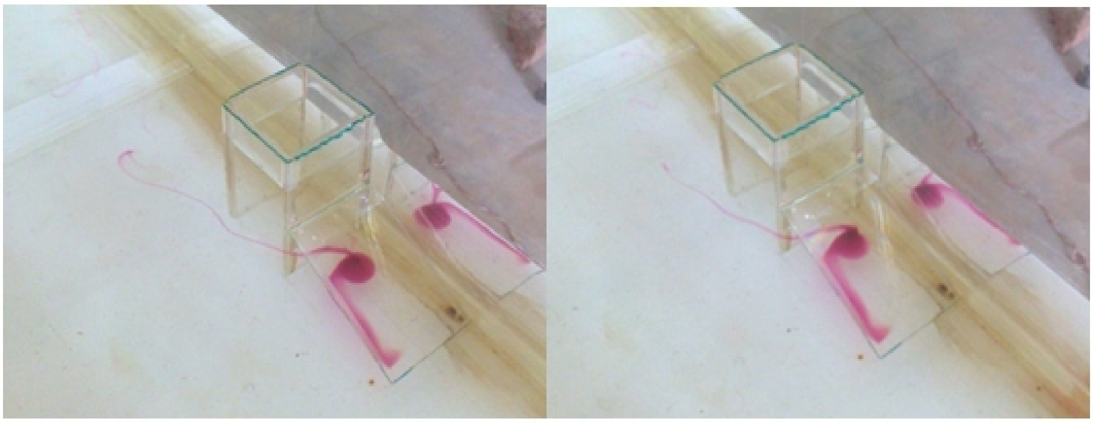

Left ***Right***

Figure 3: Pair of Stereo Images showing the Flow Modificationdue to an Inclined Plate

Table 1: Effect of Height of Inclined Plate on Scour Protection

L = 7cm, W = 7cm, B = 60cm, y = 14cm, v = 24cm/s, Fr = 0.20, α =45°

Sr. No.	Setup	Protection	z/L	y_{sm} (cm)	y_{plate} (cm)	Y_{sm}/L	Performance Potential
1	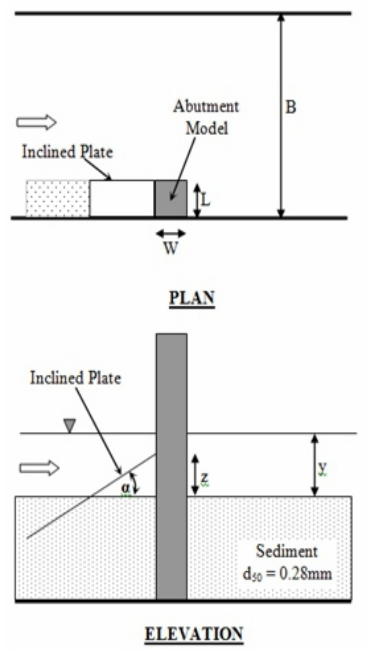	Unprotected	Unprotected	9.83	-	1.404	-
2		Protected	0	5.6	5.6	0.800	43.03
3		Protected	0.5	3.41	5.71	0.487	65.31
4		Protected	1	2.87	6.07	0.410	70.80
5		Protected	1.5	3.07	6.37	0.439	68.77
6		Protected	2	3.22	6.22	0.460	67.24
7		Protected	2.5	3.3	6.3	0.471	66.43

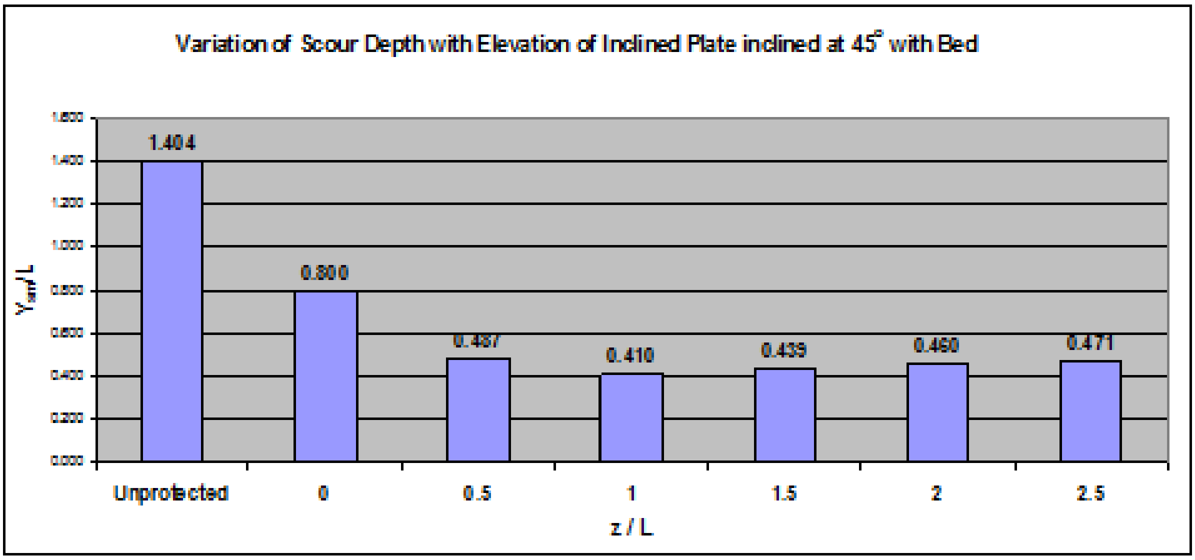

Figure 4: Effect of Height of Inclined Plate on Scour Depth

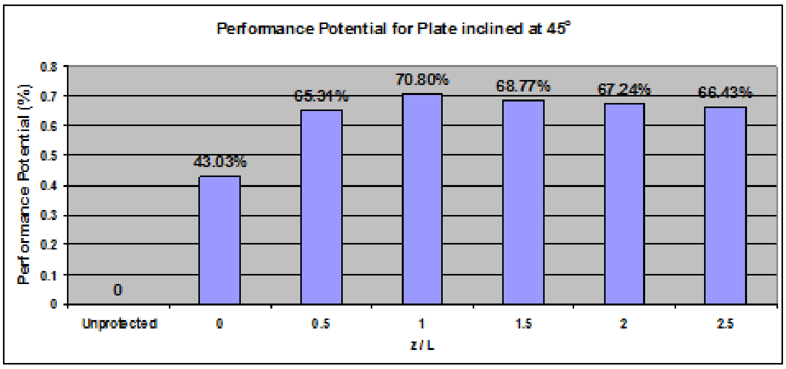

Figure 5: Effect of Height of Inclined Plate on Performance Potential

4. Effect of Angle of Inclination of Inclined Plate

The inclined plate as used in previous series was installed at five different inclinations i.e. 15˚, 30˚, 45˚, 60˚ and 75˚ with horizontal for two different heights i.e. z = 1.0L and z = 2.0L. The maximum scour depths have been presented in Table 2. Figure 6 (a and b) presents the effect of inclination of inclined plate on non-dimensionalized maximum scour depth (Y_{sm} / L) of abutment and Figure 7 (a and b) presents the performance potential of all the configurations tested in this series of experiments.

For z = 1.0L, the inclined plates were found capable of providing scour reduction ranging from a minimum of 66.73% for α = 15˚ to a maximum of 70.80% for α = 45˚, with a marginally low performance of 70.70% for α = 30˚.

For z = 2.0L, the inclined plates offered scour reduction ranging from a minimum of 63.99% for α = 30˚ to a maximum of 76.40% for α = 75˚, with a marginally close value of performance of 74.97% for α = 60˚.

Since the plates take the effect of oncoming flow as solid shields, scouring is also observed at their interaction junction with sediment. Larger angles of inclination bring the bottom of inclined plate near to the abutment and hence the scour hole at the plate may endanger the abutment. Keeping in view the scour around inclined plate itself, it is recommended that an inclined plate be installed at an angle of inclination of 30˚ to 45˚ with height z = 1.0L. This arrangement offers nearly 70% of scour reduction as compared to an unprotected abutment. Also, this arrangement keeps the scour hole of the plate away from the abutment.

5. Conclusions:

Inclined plate is a very effective scour reduction device. Variation of two parameters that were tried during the present study do not seem to have much effect on the scour potential. Therefore, presence of an inclined plate within a broad range of angles and elevations is significant in reducing scour around an abutment. Scour Protection of the order of 70% can be achieved.

Table 2: Effect of Angle of Inclination of Inclined Plate on Scour Protection

L = 7cm, W = 7cm, B = 60cm, y = 14cm, v = 24cm/s, Fr = 0.20

Sr. No.	Setup	Protection	α (degrees)	z/L = 1				z/L = 2			
				y_{sm} (cm)	y_{plate} (cm)	Y_{sm}/L	Performance Potential	y_{sm} (cm)	y_{plate} (cm)	Y_{sm}/L	Performance Potential
1	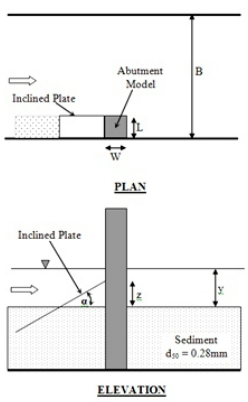	Unprotected	Unprotected	9.83	-	1.404	-	9.83	-	1.404	-
2		Protected	15˚	3.27	3.37	0.467	66.73	2.8	2.8	0.400	71.52
3		Protected	30˚	2.88	4.58	0.411	70.70	3.54	4.64	0.506	63.99
4		Protected	45˚	2.87	6.07	0.410	70.80	3.22	6.22	0.460	67.24
5		Protected	60˚	3.11	5.21	0.444	68.36	2.46	5.06	0.351	74.97
6		Protected	75˚	3.24	5.14	0.463	67.04	2.32	5.82	0.331	76.40

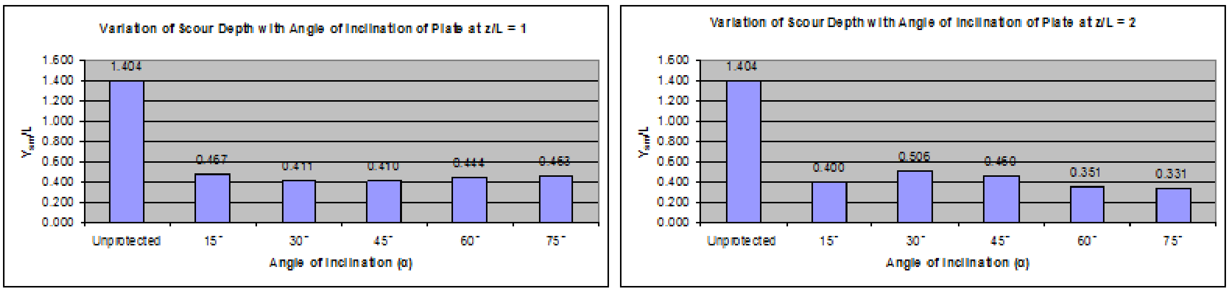

(a) **(b)**

Figure 6: Effect of Angle of Inclination of Inclined Plate on Scour Depth (a) at z/L = 1, (b) at z/L = 2

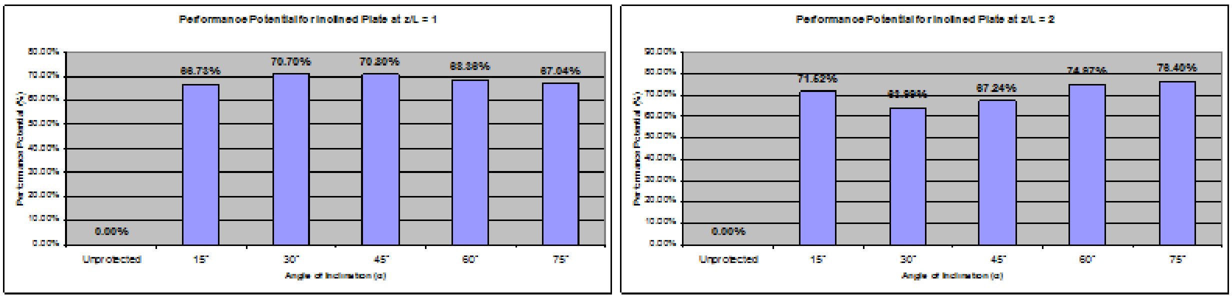

(a) **(b)**

Figure 7: Effect of Angle of Inclination of Inclined Plate on Performance Potential (a) at z/L = 1, (b) at z/L = 2

References

Ahmed F. and Rajaratnam N. (2000), "Observations on Flow around Bridge Abutment," Journal of Engineering Mechanics, ASCE, Vol. 126, No. 1, January, 2000. pp 51-59.
Ballegooy S.V. (2005), "Bridge Abutment Scour Countermeasures," PhD Thesis, University of Auckland, 2005
Barbhuiya A. K. and Dey S (2003), "Vortex Flow Field in a Scour Hole around Abutments," International Journal of Sediment Research, Vol. 18, No. 4, 2003, pp. 310-326.
Barbhuiya A.K. and Dey S. (2004), "Local Scour at Abutments: A Review," Sadhana Vol. 29, Part 5, October 2004, pp. 449–476.
Barkdoll B. D, Melville B. W. and Ettema R. (2006), "A Review of Bridge Abutment Scour Countermeasures", Proceedings of the 2006 World Environment and Water Resources Congress, May 21-25, 2006, Omaha, Nebraska.
Breusers H.N.C. and Raudkivi A.J. (1991), "Scouring", Hydraulic Structures Design Manual No. 2, A.A. Balkema Rotterdom Brookfield.
Coleman S.E, Lauchlan C.S. and Melville B.W. (2003), "Clear-Water Scour Development at Bridge Abutments," Journal of Hydraulic Research, Vol. 41, No. 5, 2003, pp 521-531.
Crawfis R.A, Shen H.W. and Max N. (2000), "Flow Visualization Techniques for CFD using Volume Rendering," 9th. International Symposium on Flow Visualization, Heriot-Watt University, Edinburgh, Scotland, UK.
Dey S. and Barbhuiya A.K. (2005c), "Flow Field at a Vertical-Wall Abutment," Journal of Hydraulic Engineering, ASCE, Vol. 131, No. 12, December 1, 2005, pp 1126-1135.
Gangadharaiah T, Setia B. and Muzzammil M. (2000), "Flow Visualization in Hydraulic Engineering", Proceedings of the International Symposium on Recen Advances in Experimental Fluid Mechanics, December 18-20, 2000, Indian Institute of Technology, Kanpur, India, pp 341-359.
Gangadharaiah T, Mamgain P, Srinivas N and Kapil M. (2001), "Scour Protection around Abutment Models", National Conference on Hydraulics and Water Resources, HYDRO-2001, Central Water and Power Station, Pune, India, 6-7 December 2001, pp 393-400.
Kline S.J. (1969), "Film Notes for Flow Visualization", National Committee for Fluid Mechanics Films, No. 21607, 1969.
Laursen E M. and Toch A, (1956), "Scour around Bridge Piers and Abutments", Bulletin No. 4, Iowa Highway Research Board, May 1956.
Li H, Kuhnle R.A. and Barkdoll B.D. (2006), "Countermeasures against Scour at Abutments," Research Report No. 49, Channel and Watershed Processes Research Unit, National Sedimentation Laboratory, USDA Agricultural Research Service, Oxford, Mississippi 38655, January, 2006
Melville B.W. (1988), "Scour at Bridge Sites", Chapter 15, Civil Engineering Practice, Hydraulics-Mechanics, Edited by Cheremisinoff et al, Technomic Publishing Company, USA.
Melville B. W. (1997), "Pier and Abutment Scour: Integrated Approach", Journal of Hydraulic Engineering, ASCE, Vol. 123. No.2, February, 1997, pp 125-136.
Sarda V.K. (2010), "Protection of Bridge Abutments from Scour," Journal of Indian Water Resources Society, Vol. 30, No. 1, January 2010, pp 1-9.
Setia B. (1997), "Scour around Bridge Piers: Mechanism and Protection", PhD. Thesis, Department of Civil Engineering, Indian Institute of Technology, Kanpur, India.
Yanmaz A.M. and Celebi T. (2004), "A Reliability Model for Bridge Abutment Scour", Turkish Journal of Engineering and Environmental Sciences, Vol. 28, pp 67-83.

Estimation Of Scour Depth Downstream Of An Apron Under 2D Horizontal Jets

M Aamir,[1] Z Ahmad [2]
[1] Ph.D. Student, Department of Civil Engineering, Indian Institute of Technology Roorkee, Roorkee-247667, India
[2] Professor, Department of Civil Engineering, Indian Institute of Technology Roorkee, Roorkee-247667, India
Email: mohdaamir.amu@gmail.com

A B S T R A C T

An analysis of laboratory data in respect of local scour downstream of a rigid apron developed under two-dimensional (2D) horizontal jets has been presented. The existing equations are also listed in the paper. Each equation has been applied to the existing data to evaluate its performance and bring forth its limitations and range of applicability. Most of the existing predictive equations are shown to perform poorly when judged against the known laboratory data. Comparison of measured scour depths with scour depths predicted by the existing equations has been plotted. The equation proposed by Dey and Sarkar (2006) performs better than others with most of the over-predicted data falling within a maximum deviation of 70% from the line of perfect agreement, with very few under-predictions. Deviation in over-predictions is found to be as high as 99% in the case of Altinbilek and Basmaci (1973) equation, whereas the equation proposed by Chatterjee et al. (1994) gives maximum deviation in under-predictions up to 95% from the line of perfect agreement.

Keywords: Scour; 2D horizontal jet; Scour depth prediction; Apron; Data analysis

1. Introduction

The phenomenon of scour downstream of hydraulic structures has engrossed the attention of many researchers due to its importance in determining the safety of hydraulic structures. Persistent scouring may lead to exposure of the foundations of these structures, thereby causing a threat to their stability. Local scour downstream of a rigid apron under 2D horizontal jets issuing from a sluice opening occurs when the erosive capacity of the jet exceeds the threshold bed shear stress for the instigation of sediment motion.

Jet issuing from under a sluice opening develops into a two-dimensional (2D) horizontal jet as it moves over the rigid apron. As soon as it encounters the erodible bed, the process of scouring is initiated. The erosive capacity of the jet is reduced as it moves further downstream of the erodible bed. Hence, a dune formation occurs at the end of the scour profile. Figure 1 shows a definition sketch of the scour hole developed under a 2D horizontal jet. In this figure, d_s = maximum equilibrium scour depth, x_s = distance from the end of apron to maximum scour depth, a = sluice opening, V = issuing jet velocity, d_t = tailwater depth, L = length of the rigid apron. Maximum scour depth depends on various parameters, viz. sluice opening, sediment size, jet Froude number, tailwater depth and length of rigid apron. Maximum scour depth increases with decrease in sluice opening and length of rigid apron, while it decreases with decrease in jet Froude number (Dey and Sarkar 2006). Maximum scour depth increases with decrease in sediment size (Ali and Neyshaboury 1991). Scour depth decreases with increase in tailwater depth up to a critical tailwater level, above which there is again an increase in the scour depth (Dey and Sarkar 2006).

Equations have been proposed by various investigators to predict the maximum scour depth like Valentin (1967), Altinbilek and Basmaci (1973), Chatterjee et al. (1994), Aderibigbe and Rajaratnam (1998), Lim and Yu (2002), Sarkar and Dey (2005), and Dey and Sarkar (2006). In this paper, an analysis of laboratory data for local scour depth developed under 2D horizontal jets has been presented. Experimental data has been taken from Dey and Sarkar (2006), Verma and Goel (2005), Lim and Yu (2002), Aderibigbe and Rajaratnam (1998), Lee (1995), Chatterjee et al. (1994), Rajaratnam and Macdougall (1983), Rajaratnam (1981), and Iwagaki et al. (1965).

1.1 *Available Data*

A large number of experimental data has been published in literature in respect of 2D horizontal jets. Range of different parameters used in the present data set of 420 known laboratory data is summarized in Table 1. In this table, F = issuing jet Froude number, D_{50} = median diameter of sediment particles.

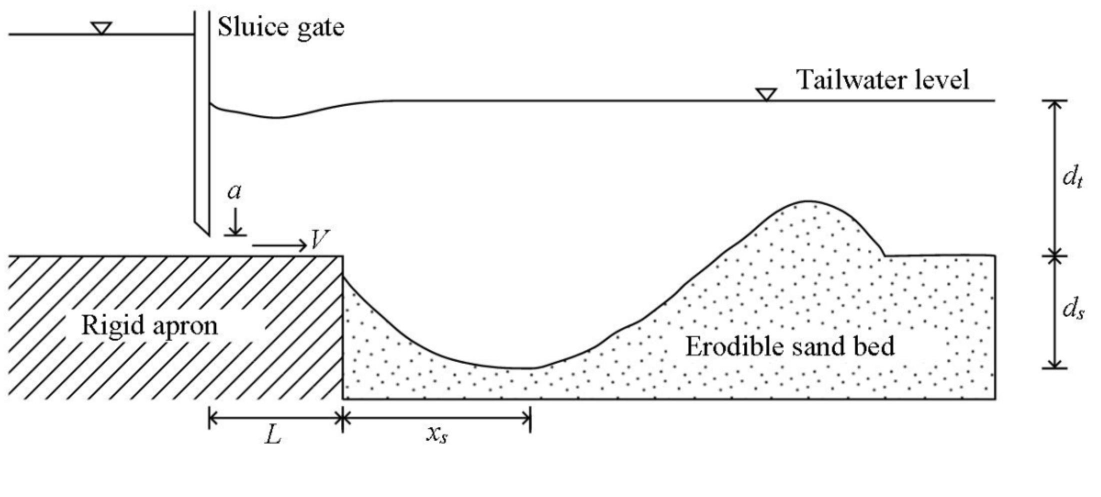

Figure 1 Definition sketch of scour hole under 2D horizontal jet

Table 1 Range of parameters for data set used in the present analysis

Investigator	Number of data	Range of parameters				
		d_s/a	F	d_t/a	D_{50}/a	L/a
Dey and Sarkar (2006)	205	2.27-8.16	2.37-4.87	6.57-13.85	0.02-0.44	26.67-55
Verma and Goel (2005)	29	0.5-4.2	1.24-4.62	3.67-29.7	0.1-0.3	9.33-60
Lim and Yu (2002)	63	0.6-20.33	1.09-7.99	10-25.4	0.08-1.64	0
Aderibigbe and Rajaratnam (1998)	30	1.32-24.4	1.21-21.54	Dec-60	0.05-1.35	0
Lee (1995)	20	1.42-5.52	0.83-2.59	5.5-9	0.07	0
Chatterjee et al. (1994)	28	0.9-4.1	1.02-5.46	5.82-15.5	0.02-0.22	13.2-33
Rajaratnam and Macdougall (1983)	12	2.1-15.83	1.56-9.3	≈ 1	0.06-0.19	0
Rajaratnam (1981)	14	3.34-31.29	0.65-3.79	15.27-106.86	0.1-0.67	0
Iwagaki et al. (1965)	19	2.65-27	1.58-9.26	25-62	0.19-0.37	-
Total	420	0.5-31.29	0.65-21.54	≈ 1-106.86	0.02-1.64	0-60

1.2 *Factors Affecting Maximum Scour Depth*

Maximum equilibrium scour depth is found to be dependent on the following parameters, as has been reported in literature:

- Jet Froude number: maximum scour depth is found to increase with increase in the issuing jet Froude number.
- Tailwater depth: increasing tailwater depth causes a reduction in the maximum scour depth up to a critical tailwater depth, after which there is an increase in the maximum scour depth.
- Sediment size: maximum scour depth decreases with an increase in sediment size, which can be represented by D_{50}.
- Length of rigid apron: maximum scour depth decreases with an increase in the length of rigid apron.

2. Scour Depth Prediction Equations

Table 2 presents the equations proposed by different investigators for prediction of maximum equilibrium scour depth. These equations have been analyzed in the present study for their performance with the available laboratory data, as listed in Table 1.

Figures 2-4 show the comparison of measured scour depths with scour depths predicted by the existing equations, by applying these equations to the data set used in this paper. Those equations considering the effect of the length of apron *L*, have been analyzed with only those sets of data for which the values of *L* were known. Hence, the data set has been primarily divided into two sets, one with known values of *L* and the other for which values of *L* are not known. The solid line in each figure is the line of perfect agreement between the observed and the predicted values of non-dimensional maximum scour depth d_s/a. The dotted line shows the percent deviation from the line of perfect agreement. It is observed that the predicted scour depths from equations proposed by Valentin (1967), Altinbilek and Basmaci (1973), and Aderibigbe and Rajaratnam (1998) deviate positively from the line of perfect agreement by more than 90%, while there is a negative deviation of 95% in case of the equation given by Chatterjee et al. (1994). Scour depth predicted from equations proposed by Lim and Yu (2002), Sarkar and Dey (2005), and Dey and Sarkar (2006) are found to give lesser deviations from the line of perfect agreement than others, the least being 70% by Dey and Sarkar (2006) equation. It is to be noted that only the data which lie within the range of applicability of a particular equation has been used to test that equation.

Figure 5 shows the comparison of measured scour depths with scour depths predicted by the equations of Chatterjee et al. (1994), Aderibigbe and Rajaratnam (1998), Lim and Yu (2002), and Dey and Sarkar (2006) with their own laboratory data. It is obvious that the deviation in these cases is much less than that in the case of application on the complete data set available. However, the equations of Aderibigbe and Rajaratnam (1998) and Lim and Yu (2002) still give large over-predictions, with percent deviations from the line of perfect agreement being 70% and 80% respectively. The data of Chatterjee et al. (1994) and Dey and Sarkar (2006) lie within an error of ±10% and ±20% respectively, which means that these equations perform much better than others when tested against their own data set.

Table 2 Scour depth prediction equations used in the present analysis

Investigator	Equation
Valentin (1967)	$\log\left(\frac{d_s}{a}\right) = \frac{F-2}{4.7} - 0.55\log\left(\frac{D_{90}}{a}\right)$; where D_{90} = particle size for which 90% are finer by weight
Altinbilek and Basmaci (1973)	$\frac{d_s}{a} = \left(\frac{a}{D_{50}}\tan\phi\right)^{0.5} F_d^{1.5}$; where $F_d = V/(\Delta g D_{50})^{0.5}$, where V = issuing jet velocity, g = acceleration due to gravity, $\Delta = s$-1, s = relative density of sediment; ϕ = angle of repose
Chatterjee et al. (1994)	$\frac{d_s}{a} = 0.775F$
Aderibigbe and Rajaratnam (1998)	$\frac{d_s}{a} = 3.35F_{d(95)} - 6.11$; where $F_{d(95)}$ = densimetric Froude number based on D_{95}
Lim and Yu (2002)	$\frac{d_s}{a} = 1.04F_d^{1.47}\sigma_g^{-0.69}\left(\frac{D_{50}}{a}\right)^{0.33}K_L'$; where K_L' = factor to account for the effects of an apron downstream from the outlet, which is given by $K_L' = e^{-0.004F_d^{-0.35}\sigma_g^{-0.5}\left(\frac{D_{50}}{a}\right)^{-0.5}\left(\frac{L}{a}\right)^{1.4}}$; σ_g = geometric standard deviation
Sarkar and Dey (2005)	$\frac{d_s}{a} = 0.42F_d^{0.49}\left(\frac{L}{a}\right)^{-0.36}\left(\frac{d_t}{a}\right)^{1.08}$
Dey and Sarkar (2006)	$\frac{d_s}{a} = 2.59F_d^{0.94}\left(\frac{L}{a}\right)^{-0.37}\left(\frac{d_t}{a}\right)^{0.16}\left(\frac{D_{50}}{a}\right)^{0.25}$

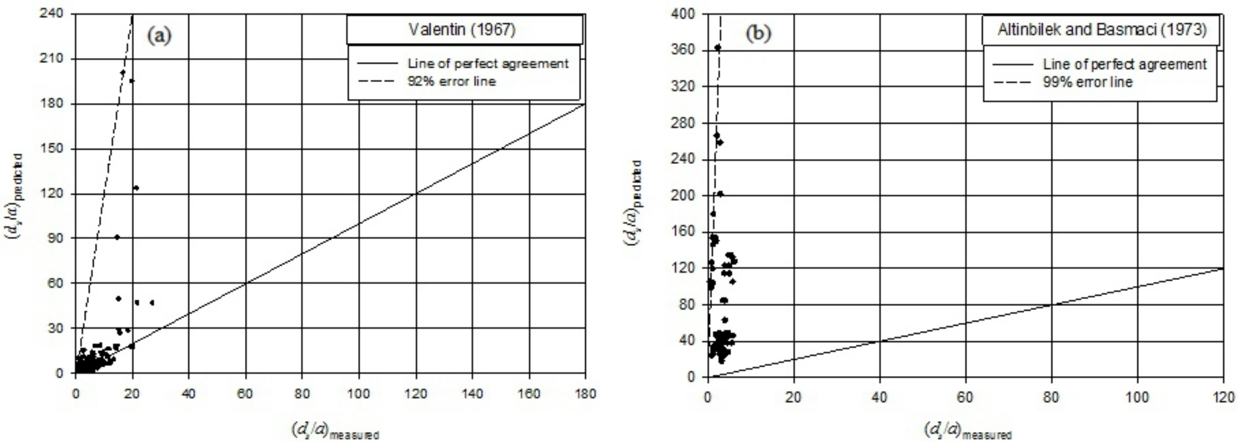

Figure 2 Comparison of measured scour depths with scour depths predicted by the equations of (a) Valentin (1967); (b) Altinbilek and Basmaci (1973)

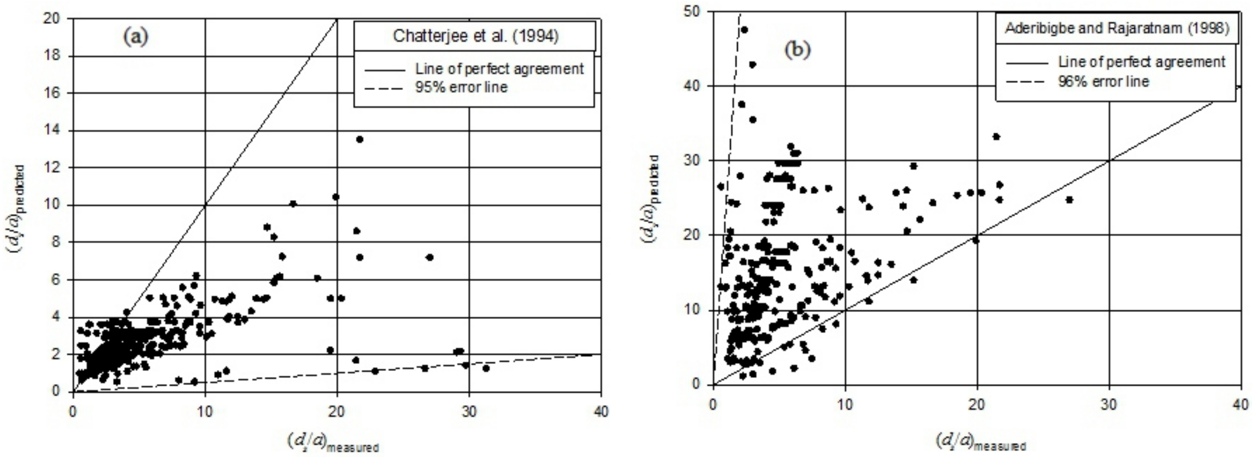

Figure 3 Comparison of measured scour depths with scour depths predicted by the equations of (a) Chatterjee et al. (1994); (b) Aderibigbe and Rajaratnam (1998)

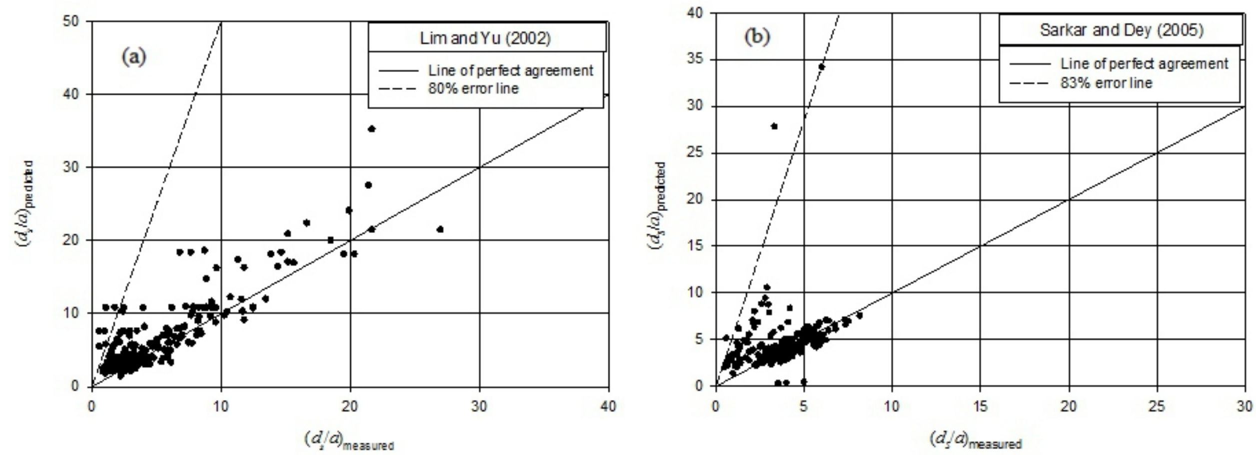

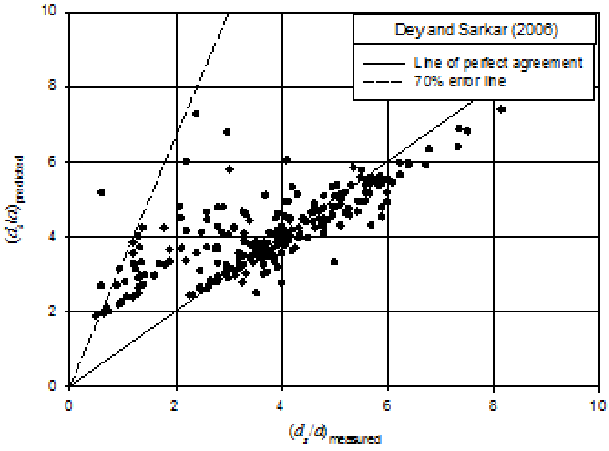

Figure 4 Comparison of measured scour depths with scour depths predicted by the equations of (a) Lim and Yu (2002); (b) Sarkar and Dey (2005); (c) Dey and Sarkar (2006)

It is to be noted that the equation proposed by Chatterjee et al. (1994) considers the maximum scour depth to be dependent upon the issuing jet Froude number only, neglecting the effect of other parameters. On the other hand, equation proposed by Dey and Sarkar (2006) takes into account the effect of a number of parameters on the maximum scour depth, viz. densimetric Froude number F_d, length of the rigid apron L, tailwater depth d_t, and sediment size represented by D_{50}. This increases the accuracy of the predicted scour depth since a larger number of parameters are considered for the prediction of maximum scour depth. However, the applicability of this equation also becomes limited to a certain range, as in this case, the range of applicability being $6.57 \leq (d_t/a) \leq 13.85$ and $(L/a) > 26$, as mentioned by Dey and Sarkar (2006). Less number of parameters involved in the equation of Chatterjee et al. (1994) makes it applicable to a wider range.

A close examination, however, shows that the Chatterjee et al. (1994) equation under-predicts the scour depth in most of the cases when tested with the available data, the maximum deviation from the line of perfect agreement being as high as 95%, which makes it unsafe to apply this equation in general. The Dey and Sarkar (2006) equation, on the other hand, generally over-predicts the scour depth when tested with the available data, the maximum deviation from the line of perfect agreement being 70% only. Thus, it can be well stated that the Dey and Sarkar (2006) equation has a wider range of applicability on the available data.

3. Error Analysis

Table 3 presents the percentage of under-predictions and the percentage of over-predictions by applying the existing equations to the data set used in this paper. Each equation was tested against the data which fall within the range of applicability of that equation. However, the equation proposed by

Chatterjee et al. (1994) was tested against the complete data set, since it takes into consideration only the effect of jet Froude number for the calculation of maximum scour depth and no other constraints have been specified for the applicability of this equation. Hence, a large number of under-predictions is observed in this case. The equations given by Valentin (1967) and Lim and Yu (2002) also feature a significant number of under-predictions. Aderibigbe and Rajaratnam (1998) equation has a significant number of over-predictions more than 200%, whereas Altinbilek and Basmaci (1973) predicts unrealistically high scour depth, giving over-predictions greater than 200% for the complete data set applied to it. Sarkar and Dey (2005) and Dey and Sarkar (2006) equations outperform others, in which case the number of over-predictions is significantly less. However, a large number of under-predictions is given by these equations also, but most of them are less than 25%. As regards the overall performance of existing prediction equations, it can be stated that the equation proposed by Dey and Sarkar (2006) shows a consistent trend for most of the data, and hence can be regarded as superior to other existing equations within its range of applicability.

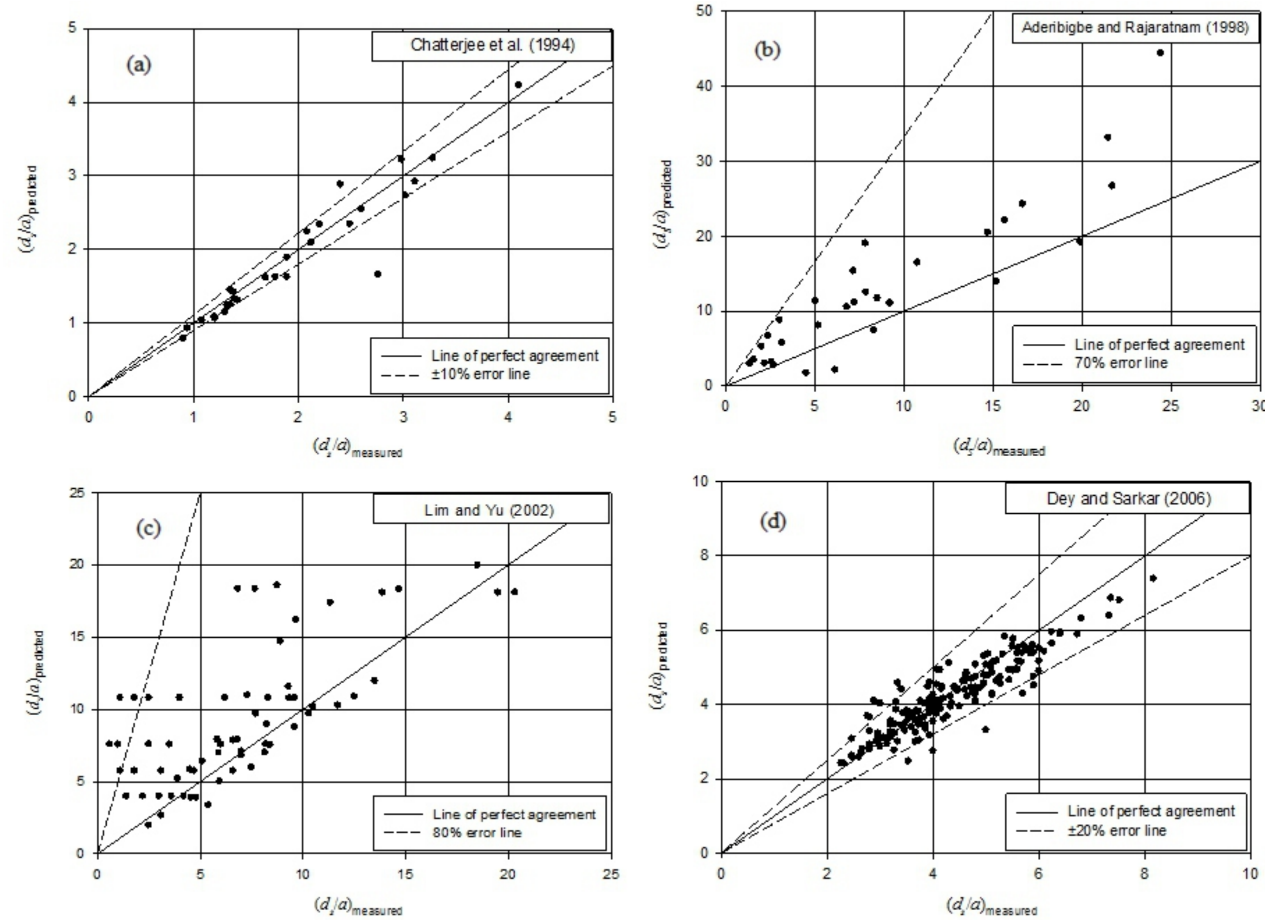

Figure 5 Comparison of measured scour depths with scour depths predicted by the equations of (a) Chatterjee et al. (1994); (b) Aderibigbe and Rajaratnam (1998); (c) Lim and Yu (2002); (d) Dey and Sarkar (2006) with their own laboratory data

Table 3 Comparison of measured scour depths with scour depths predicted using existing equations

Investigator	Percentage of over-predictions			Percentage of under-predictions		
	greater than 200%	greater than 100%	greater than 50%	Total under-predictions	greater than 25%	greater than 50%
Dey and Sarkar (2006)	6.7	13.7	19.8	40.6	1	0
Sarkar and Dey (2005)	11.5	15.7	21.1	39.6	5.4	1
Lim and Yu (2002)	9	19.1	33.7	26.1	5	0
Aderibigbe and Rajaratnam (1998)	63.2	77.4	86.6	4.6	1.6	1.3
Chatterjee et al. (1994)	0.4	1.5	3	89	70.5	24
Altinbilek and Basmaci (1973)	100	100	100	0	0	0
Valentin (1967)	6.5	18.1	42.2	21.9	12.2	1.4

4. Conclusions

The following conclusions are drawn from this study:

- Local scour depth caused by 2D horizontal jets is dependent on jet Froude number, tailwater depth, length of the rigid apron, sluice opening and sediment size.
- Most of the existing predictive equations perform poorly when compared with the available data.
- Equation proposed by Dey and Sarkar (2006) performs better than others when judged against the available laboratory data, with percentage of over-predictions (greater than 200%) being 6.7% only.
- Equation proposed by Chatterjee et al. (1994) generally under-predicts the maximum scour, with total under-predictions being 89%.
- Altinbilek and Basmaci (1973) equation predicts unrealistically high scour depth, giving over-predictions greater than 200% for the complete data set.
- The equations given by Valentin (1967) and Lim and Yu (2002) also feature a significant number of under-predictions.

References

Aderibigbe, O., and Rajaratnam, N. (1998). Effect of sediment gradation on erosion by plane turbulent wall jets. Journal of Hydraulic Engineering, 124(10), 1034–1042.

Ali, K. H. M., and Neyshaboury, A. A. S. (1991). Localized scour downstream of a deeply submerged horizontal jet. Proceedings of the Institution of Civil Engineers (London), 91(2), 1-18.

Altinbilek, H. D., and Basmaci, Y. (1973). Localized scour at the downstream of outlet structures. Proceedings of the 11th Congress on Large Dams, International Commission of Large Dams, Madrid, Spain, 105–121.

Chatterjee, S. S., Ghosh, S. N., and Chatterjee, M. (1994). Local scour due to submerged horizontal jet. Journal of Hydraulic Engineering, 120(8), 973–992.

Dey, S., and Sarkar, A. (2006). Scour downstream of an apron due to submerged horizontal jets. Journal of Hydraulic Engineering, 132(3), 246–257.

Iwagaki, Y., Tsuchiya, Y., and Imamura, M. (1965). Studies of the local scour from flows downstream of an outlet (1). Disaster Prevention Research Institute, Kyoto Univ., Kyoto, Japan, 363–377.

Lee, W. W. L. (1995). Erosion downstream of a sluice gate. Nanyang Technological University, Singapore.

Lim, S. Y., and Yu, G. (2002). Scouring downstream of sluice gate. Proceedings of the 1st International

Conference on Scour of Foundations, Texas Transportation Institute, College Station, TX, 1, 395–409.
Rajaratnam, N. (1981). Erosion by plane turbulent jets. Journal of Hydraulic Research, 19(4), 339–358.
Rajaratnam, N., and Macdougall, R. K. (1983). Erosion by plane wall jets with minimum tail water. Journal of Hydraulic Engineering, 109(7), 1061–1064.
Sarkar, A., and Dey, S. (2005). Scour downstream of aprons caused by sluices. Proceedings of the Institution of Civil Engineers, 158(2), 55–64.
Valentin, F. (1967). Considerations concerning scour in the case of flow under gates. Proceedings of the 12th IAHR Congress, Madrid, Spain, 3, 92–96.
Verma, D. V. S., and Goel, A. (2005). Scour downstream of a sluice gate. ISH Journal of Hydraulic Engineering, 11(3), 57–65.

Instructions for Authors

Essentials for Publishing in this Journal

1 Submitted articles should not have been previously published or be currently under consideration for publication elsewhere.

2 Conference papers may only be submitted if the paper has been completely re-written (taken to mean more than 50%) and the author has cleared any necessary permission with the copyright owner if it has been previously copyrighted.

3 All our articles are refereed through a double-blind process.

4 All authors must declare they have read and agreed to the content of the submitted article and must sign a declaration correspond to the originality of the article.

Submission Process

All articles for this journal must be submitted using our online submissions system. http://enrichedpub.com/ . Please use the Submit Your Article link in the Author Service area.
-

Manuscript Guidelines

The instructions to authors about the article preparation for publication in the Manuscripts are submitted online, through the e-Ur (Electronic editing) system, developed by **Enriched Publications Pvt. Ltd**. The article should contain the abstract with keywords, introduction, body, conclusion, references and the summary in English language (without heading and subheading enumeration). The article length should not exceed 16 pages of A4 paper format.

Title

The title should be informative. It is in both Journal's and author's best interest to use terms suitable. For indexing and word search. If there are no such terms in the title, the author is strongly advised to add a subtitle. The title should be given in English as well. The titles precede the abstract and the summary in an appropriate language.

Letterhead Title

The letterhead title is given at a top of each page for easier identification of article copies in an Electronic form in particular. It contains the author's surname and first name initial .article title, journal title and collation (year, volume, and issue, first and last page). The journal and article titles can be given in a shortened form.

Author's Name

Full name(s) of author(s) should be used. It is advisable to give the middle initial. Names are given in their original form.

Contact Details

The postal address or the e-mail address of the author (usually of the first one if there are more Authors) is given in the footnote at the bottom of the first page.

Type of Articles

Classification of articles is a duty of the editorial staff and is of special importance. Referees and the members of the editorial staff, or section editors, can propose a category, but the editor-in-chief has the sole responsibility for their classification. Journal articles are classified as follows:

Scientific articles:

1. Original scientific paper (giving the previously unpublished results of the author's own research based on management methods).

2. Survey paper (giving an original, detailed and critical view of a research problem or an area to which the author has made a contribution visible through his self-citation);

3. Short or preliminary communication (original management paper of full format but of a smaller extent or of a preliminary character);

4. Scientific critique or forum (discussion on a particular scientific topic, based exclusively on management argumentation) and commentaries. Exceptionally, in particular areas, a scientific paper in the Journal can be in a form of a monograph or a critical edition of scientific data (historical, archival, lexicographic, bibliographic, data survey, etc.) which were unknown or hardly accessible for scientific research.

Professional articles:

1. Professional paper (contribution offering experience useful for improvement of professional practice but not necessarily based on scientific methods);
2. Informative contribution (editorial, commentary, etc.);
3. Review (of a book, software, case study, scientific event, etc.)

Language

The article should be in English. The grammar and style of the article should be of good quality. The systematized text should be without abbreviations (except standard ones). All measurements must be in SI units. The sequence of formulae is denoted in Arabic numerals in parentheses on the right-hand side.

Abstract and Summary

An abstract is a concise informative presentation of the article content for fast and accurate Evaluation of its relevance. It is both in the Editorial Office's and the author's best interest for an abstract to contain terms often used for indexing and article search. The abstract describes the purpose of the study and the methods, outlines the findings and state the conclusions. A 100- to 250-Word abstract should be placed between the title and the keywords with the body text to follow. Besides an abstract are advised to have a summary in English, at the end of the article, after the Reference list. The summary should be structured and long up to 1/10 of the article length (it is more extensive than the abstract).

Keywords

Keywords are terms or phrases showing adequately the article content for indexing and search purposes. They should be allocated heaving in mind widely accepted international sources (index, dictionary or thesaurus), such as the Web of Science keyword list for science in general. The higher their usage frequency is the better. Up to 10 keywords immediately follow the abstract and the summary, in respective languages.

Acknowledgements

The name and the number of the project or programmed within which the article was realized is given in a separate note at the bottom of the first page together with the name of the institution which financially supported the project or programmed.

Tables and Illustrations

All the captions should be in the original language as well as in English, together with the texts in illustrations if possible. Tables are typed in the same style as the text and are denoted by numerals at the top. Photographs and drawings, placed appropriately in the text, should be clear, precise and suitable for reproduction. Drawings should be created in Word or Corel.

Citation in the Text

Citation in the text must be uniform. When citing references in the text, use the reference number set in square brackets from the Reference list at the end of the article.

Footnotes

Footnotes are given at the bottom of the page with the text they refer to. They can contain less relevant details, additional explanations or used sources (e.g. scientific material, manuals). They cannot replace the cited literature.
The article should be accompanied with a cover letter with the information about the author(s): surname, middle initial, first name, and citizen personal number, rank, title, e-mail address, and affiliation address, home address including municipality, phone number in the office and at home (or a mobile phone number). The cover letter should state the type of the article and tell which illustrations are original and which are not.

Notes: